High-Spin Isomer and Level Structure in ^〈145〉Sm

小田原, 厚子
九州大学理学研究科物理学専攻

https://doi.org/10.11501/3075395

出版情報：九州大学, 1993, 博士（理学）, 課程博士
バージョン：
権利関係：

High-Spin Isomer and Level Structure in ^{145}Sm

小田原　厚子

High-Spin Isomer and Level Structure in ^{145}Sm

Atsuko Odahara

Department of Physics, Faculty of Science, Kyushu University,
Fukuoka, 812, Japan

22 December 1993

Contents

Abstract

A high-spin isomer in ^{145}Sm was discovered by using inverse kinematic reactions, ^{20}Ne(^{136}Xe,α7n)^{145}Sm and ^{16}O(^{136}Xe,7n)^{145}Sm. The half life was determined to be 0.96 μsec. Sixty-five γ-rays were identified by the $\gamma\gamma$-coincidence measurements to belong to the isomer decay. The low-lying level scheme of ^{145}Sm was established in detail by the in-beam γ-ray measurements using the ^{139}La(^{10}B,4n)^{145}Sm reaction. A complex decay scheme of this isomer was constructed by using the data obtained from the ^{136}Xe induced reactions, combining the informations of low-lying states mentioned above. The excitation energy of this isomer was determined to be 8.8 MeV. The $\gamma\gamma$-coincidence measurement using the ^{138}Ba(^{13}C,6n)^{145}Sm reaction was also performed. Based on this information, the level scheme above the high-spin isomer was extended up to the state at 14.6 MeV. A γ-ray angular distribution measurement using the same reaction with pulsed beam was carried out and was used to assign a spin value of each level.

Low-lying states in ^{145}Sm were interpreted to originate from a single neutron coupled to the ^{144}Sm core excitation. Experimental yrast states were compared with a calculation of a deformed independent particle model (DIPM). A configuration of the high-spin isomer was deduced by the DIPM calculation to be $\{\pi h_{11/2}{}^2\nu(f_{7/2}h_{9/2}i_{13/2})\}_{49/2^+}$.

1. Introduction

Isomers in nuclei have been known since Hahn discovered an isomer of ^{234}Pa in 1921. This kind of isomerism is caused by the transitions of low energies or high multipolarities. These isomers were observed in the region of low excitation energy or near ground states. Later, K-isomers and fission isomers of different characters were discovered. The former stems from the K-selection rule, while the latter arises from a difference of shapes between the isomer and the ground state. In 1970s, the search of isomers in high-spin region was carried out. These isomers are called high-spin isomers or yrast traps.

The high-spin isomers were predicted by Bohr and Mottelson[1]. Since the states with the lowest energies for given angular momenta are called yrast states, these high-spin isomers are named yrast traps. In high-spin region, the Coriolis force overcomes the pairing force and consequently the superfluidity of nuclei disappears. The angular momenta of individual particles become to be aligned along the symmetry axis and the shape changes from prolate (or spherical) to oblate. Excitation energies of yrast states at high spin can be estimated as a sum of those of the single-particle orbits. In this regime, a yrast line is on average proportional to I(I+1) with a coefficient given by the classical rigid-body moment of inertia. However, the excitation energy of each state is irregular with respect to the straight line because of the single-particle characters. When the irregularity is large and the neighbouring yrast state of one or two units less spin has lower slightly or higher in the excitation energy, the electromagnetic transition is reduced. Therefore this state becomes to be a high-spin isomer.

The experimental search of yrast traps was carried out for the first time by Pedersen et al.[2]. More than 100 compound nuclei in the region between Ba and Pb were investigated using ^{40}Ar, ^{50}Ti and ^{65}Cu beams. They measured the γ-ray multiplicities and the total energies using a recoil catcher method. Twenty-two

compound nuclei in the region of $64 \leq Z \leq 71$ and $82 \leq N \leq 88$ were observed to decay to the nuclei with high-spin isomers. However, they could not determine in most cases of the nuclei which have high-spin isomers. Nuclei with the high-spin isomers were identified only in the cases of ^{146}Gd and ^{147}Gd based on the observations of discrete γ-rays known previously in the low-spin region. Although the results gave half lives and the ranges of spin values of the isomers, their exact excitation energies and decay schemes could not be determined.

Following the experimental discoveries, detailed calculations were performed using both of the microscopic and the macroscopic-microscopic method. The former method was developed by Jülich[3-4] group and the latter was made by the groups of Lund-Warsaw[5-9], Dubna-Rossendorf[10-11] and Copenhargen[12-14]. The former group calculated the deformation energy using a many-body model Hamiltonian and trial wave functions representing the different shapes. It was discussed that the high-spin isomers were caused by the energy gain originated from the maximum overlap of the nucleonic wave functions by alignment (MONA effect) of the single-particle angular momenta outside the closed shell. Due to this effect, the particle wave functions concentrate near the equator at the beginning of a shell. The latter method is called to be a deformed independent particle model (DIPM). Energies of single-particle orbits were calculated as a function of a shape using a modified oscillator (MO) or a deformed Woods-Saxon potential. The energy surface was calculated involving Strutinsky shell correction method. The total angular momentum of nucleus consists of the sum of single-particle angular momenta along the symmetry axis. Searches for yrast traps were performed within these theoretical frameworks assuming the axially symmetric oblate shapes.

The nucleus ^{147}Gd was investigated experimentally and theoretically in detail. The decay scheme of a 510 nsec high-spin isomer was reported[15-16]. The configuration of this isomer was calculated to be $\{\pi(h_{11/2}{}^2)_{10^+}\nu(f_{7/2}h_{9/2}i_{13/2})_{29/2^+}\}_{49/2^+}$ (ref.14). The experimental g-factors[17]

supported the configuration obtained by the DIPM calculation. The deformation parameter of this state was determined to be -0.19 by the measurement of the static quadrupole moment[18]. At present, the level scheme was reported up to the state at 18.7 MeV and transitions were favored to have the single-particle characters[19]. Recently, the two discrete superdeformed bands were also found in ^{147}Gd by Strasbourg group[20].

In this work, the nucleus ^{145}Sm was studied. This nucleus is one of N=83 isotones as same as ^{147}Gd, and consists of two proton holes and one valence neutron with respect to the semi doubly closed shell nucleus ^{146}Gd. A large energy gap between the $2d_{5/2}$ and $1h_{11/2}$ single-particle orbits was proved by the excitation energies of the lowest 3^- and 2^+ states[21–22]. The excited states of the neighbouring nuclei are interpreted to stem from particle-hole excitations and two nucleon interactions. In low-spin region, the states in ^{145}Sm and ^{147}Gd are well reproduced by the empirical single-particle energies. However, the high-spin states of ^{145}Sm were not studied enough to compare with those of ^{147}Gd.

In this work, the search of high-spin isomers (yrast traps) in A $\sim$ 150 region was carried out using a recoil catcher system, and a new isomer in ^{145}Sm was found. The level scheme was constructed up to the state at 14.6 MeV beyond the $49/2^+$ isomer at 8.8 MeV, based on the $\gamma\gamma$-coincidence measurement. The spin assignments were tentatively given by using the angular distribution data.

Previously, the nucleus ^{145}Sm was studied by means of in-beam γ-ray spectroscopy using the (α,xn) reaction. The $\gamma\gamma$-coincidence and conversion electrons were measured by Piiparinen et al.[26]. The level scheme was established up to the $25/2^+$ state at 3.5 MeV. A shell model analysis was carried out using the excitation energies of one- and two-particle (or hole) states of neighbouring nuclei. The states were interpreted as a $f_{7/2}$ valence neutron coupled to the ^{144}Sm particle-hole excitations. The other in-beam studies using the ^{144}Nd(α,3n)^{145}Sm reactions were also reported [27–28]. The low-lying states in ^{145}Sm were also

studied by the β-decay of ^{145}Eu[29]. The experimental results using the ^{146}Sm(d,p)^{145}Sm[30] and ^{146}Sm(d,t)^{145}Sm[31] reactions indicated that some of the low-lying states were generated by the single neutron excitations and the particle-phonon septuplet of $\nu f_{7/2} \otimes 3^-$.

In this paper, the experimental procedures and results are described in section 2. The search of high-spin isomers in ^{145}Sm at RIKEN using a recoil catcher system is shown in section 2-1. The study of the low-lying states using Kyushu University Tandem Accelerator is given in section 2-2. The observation of the levels above the high-spin isomer and the angular distribution measurements at Japan Atomic Energy Research Institute are presented in sections 2-3 and 2-4, respectively. The construction of the level scheme of ^{145}Sm is presented in section 3. The systematics of the level energies including the neighbouring nuclei are discussed in section 4-1. The configuration assignments of low-lying states in ^{145}Sm are carried out, and experimental yrast states are compared with those calculated by DIPM[23], in section 4-2. The variation of deformation parameter β calculated using DIPM[23] is discussed in section 4-3. The average moment of inertia of ^{145}Sm and ^{147}Gd obtained by experiments are compared with rigid body values in section 4-4.

2. Experimental Procedures and Results

2-1. Search for High-Spin Isomers at RIKEN

Experiments to search for the high-spin isomers were performed at RIKEN for N=83 isotones in A$\sim$150 region. The high-spin states of ^{145}Sm were populated by the ^{16}O(^{136}Xe,7n)^{145}Sm and ^{20}Ne(^{136}Xe,α7n)^{145}Sm reactions. In the former case, the ^{136}Xe beam of 9.6 MeV/u was provided by RIKEN Ring Cyclotron and was degraded to about 7.6 MeV/u by a harvar and an aluminium foil with thickness of 4.6 and 2.0 mg/cm^2, respectively. In the latter case, the 10.0 MeV/u ^{136}Xe beam was degraded to about 8.2 MeV/u by the same foils of 4.6 and 1.4 mg/cm^2 thickness, respectively.

In order to separate the primary beam and reaction products, the gas filled recoil ion separator[32] was used. This system was consisted of a dipole and a pair of quadrupole magnets as shown in fig.2.1. The reaction products were recoiled out of the target and flied to the catcher position at the 6 m down stream through gases of a few Torr He, N_2, Ne or Ar filled in the beam line through 5 m length. After passing through these gases, the widths of charge state distributions both of the reaction products and primary beam were reduced. It was possible to separate them at the catcher position, since they had different charge states and energies. Using the ^{16}O(^{136}Xe,7n)^{145}Sm reaction, the 80 mm separation between them was obtained for their center of momenta. It was found that the filling gas worked as the target as well. As the flight time of the reaction products from the target to the catcher position was about 200 nsec, the only γ-rays emitted by the isotopes, which have isomers, and the activities with proper life time, could be observed. In this experiment, Ne-gas was used for the purpose of the filling gas as well as the target of a few mg/cm^2 thickness.

The $\gamma\gamma$-coincidence measurement was carried out. Gamma-rays were detected

by 7 HPGe detectors of 30 % efficiency with BGO compton suppression shields placed on the perpendicular plane to the beam.

Figure 2-2(a) shows the $\gamma\gamma$-coincidence spectrum gated by the 1105 keV transition in ^{145}Sm, which was previously reported as a transition between $13/2^+$ and $7/2^-$ levels. Many unknown γ-rays were observed and 65 γ-rays were identified to belong to ^{145}Sm. The lists of these γ-rays are given in Table 2-1. Since the experimental set-up allowed us to detect γ-rays only from isomers and activities, the observation of so many γ-rays of ^{145}Sm indicates the existence of a relatively long lived and high-spin isomer in ^{145}Sm. Examples of γ-ray coincidence spectra are presented in fig.2-3.

In order to determine the life time of the high-spin isomer in ^{145}Sm, the particle-γ delayed coincidence measurement was also performed using the ^{16}O(^{136}Xe,7n)^{145}Sm reaction, as was described in Ref. 33. Particles were detected by the plastic scintillator with 0.2 mm thickness set at the catcher position. The time distribution between particles and γ-rays is shown in fig.2-4. This spectrum was obtained without selecting any γ-ray, assuming that most of transitions originate from the decay of the isomer in ^{145}Sm. The life time of the high-spin isomer was determined to be $0.96^{+0.19}_{-0.15}$ μ sec.

2-2. Study of Low-Lying States in ^{145}Sm at Kyushu University

In order to investigate the low-lying states in ^{145}Sm, the experiment using the ^{139}La(^{10}B,4n)^{145}Sm reaction was carried out. The ^{10}B beam of 47 MeV was provided by Kyushu University Tandem Accelerator. The ^{139}La rolled target of 51 mg/cm^2 thickness was used and was thick enough to stop the beam in it.

Second foil stripper system[34] was used for the purpose of taking the stable beam from tandem accelerator without using the high terminal voltage. This foil

was set at 2m down stream from the center terminal. The BO^- beam of 125 nA was extracted from the sputter ion source, and changed to B^{4+} after passing through the carbon foil placed at the center terminal position. And B^{5+} beam of 7 nA was obtained after second stripper foil.

The $\gamma\gamma$-coincidence measurement was carried out. Gamma-rays were detected by 5 HPGe detectors of 30 % efficiency with BGO compton suppression shields placed at θ=0°, 30°, 55°, 90°(ϕ=0°) and θ=90°(ϕ=90°) with respect to the beam direction.

Data acquisition was carried out using CAMAC system supported by personal computer (PC-98). In this system, the auxiliary controller (Sub Create Controller) and the ring buffer memory (Event Buffer) was used to reduce the dead time with respect to high counting rate. Sub Create Controller read data both from ADC and TDC, and sent this list data with header to Event Buffer. List data, which was stored temporarily in it, were directly transported to a hard disk connected with the work station (News) by using network file system (NFS). PC-98 controlled this system and was used for the on-line monitoring.

Figure 2-2(b) displays the γ-ray spectrum in coincidence with the 1105 keV transition in ^{145}Sm. The angular momentum in the compound nucleus 26 $\hbar$ induced by this reaction is smaller than 74 $\hbar$ generated by the beam target combination used at RIKEN. Therefore the spectrum is simpler than fig.2-2(a) and gives useful information about the low-lying levels below 5 MeV in ^{145}Sm. Typical gated spectra are shown in fig.2-5. The γ-ray intensities are summarized in Table 2-1.

2-3. Search for the States above High-Spin Isomer at JAERI

In order to search for the states above the high-spin isomer in ^{145}Sm, the

experiment using the ^{138}Ba(^{13}C,6n)^{145}Sm reaction was carried out. The ^{13}C beam of 95 MeV was obtained from tandem accelerator at Japan Atomic Energy Research Institute(JAERI). The ^{138}Ba target was rolled to 22 mg/cm^2 thickness.

The $\gamma\gamma$-coincidence measurement was performed. Gamma-rays were detected by 5 HPGe detectors of 30 % efficiency with BGO compton suppression shields at angles of θ=$\pm$55°, $\pm$125°(ϕ=0°) and θ=90°(ϕ=90°) with respect to the beam.

The gate width of $\gamma\gamma$-timing was set to be 2 μsec, because the life time of high-spin isomer in ^{145}Sm is 0.96μ sec.

Figure 2-6(b) gives $\gamma\gamma$-prompt projection spectrum. In order to investigate the transitions between levels above the high-spin isomer, figure 2-6(a) displays the sum of 12 different $\gamma\gamma$-preprompt spectra gated by strong delayed γ-rays assigned to ^{145}Sm. The feeding γ-rays above the $49/2^+$ isomer were selected from comparison between two spectra. The coincidence spectrum gated by the 1195 keV γ-ray, which was assigned to feed the isomer, is presented in fig. 2-7. Consequently, 12 γ-rays were found as transitions above the isomer in ^{145}Sm. The characteristics of these γ-rays are listed in Table 2-2.

2-4. Angular Distributions

The experiment using the ^{138}Ba(^{13}C,6n)^{145}Sm reaction was performed at JAERI using the pulsed 98 MeV ^{13}C beam with 50 nsec bursts separated by 250 nsec. The ^{138}Ba target was rolled to a 10 mg/cm^2 thickness.

The $\gamma\gamma$-coincidence and angular distribution measurements were carried out. Gamma-rays were detected by 6 HPGe detectors of 30 % efficiency with BGO compton suppression shields located at angles of θ= $-$125°, $-$90°, $-$35°, 60°, 150°(ϕ=0°) and θ=90°(ϕ=90°) with respect to the beam.

Figure 2-8 displays γ-ray singles spectra both of in-beam and off-beam. The

γ-rays which belong to the isomer decay appear to be enhanced in the off-beam spectrum. These γ-rays in this spectrum show the isotropic distributions. Therefore, the efficiency calibration of each Ge detectors positioned at 30°, 60° and 90° angles was performed by using 5 γ-rays below the 880 nsec isomer in ^{144}Sm appeared in the same spectrum. Based on this calibration curve, the data from the different angles were normalized. The efficiency-corrected intensity for each γ-ray was fitted to a formula,

$$W(\theta)=A_0+A_2P_2(\cos\theta). \qquad (1)$$

Angular distribution of each γ-ray is shown in fig.2-9. The A_2/A_0 coefficients are listed in Table 2-3. Graphical presentation of these coefficients is displayed in fig.2-10.

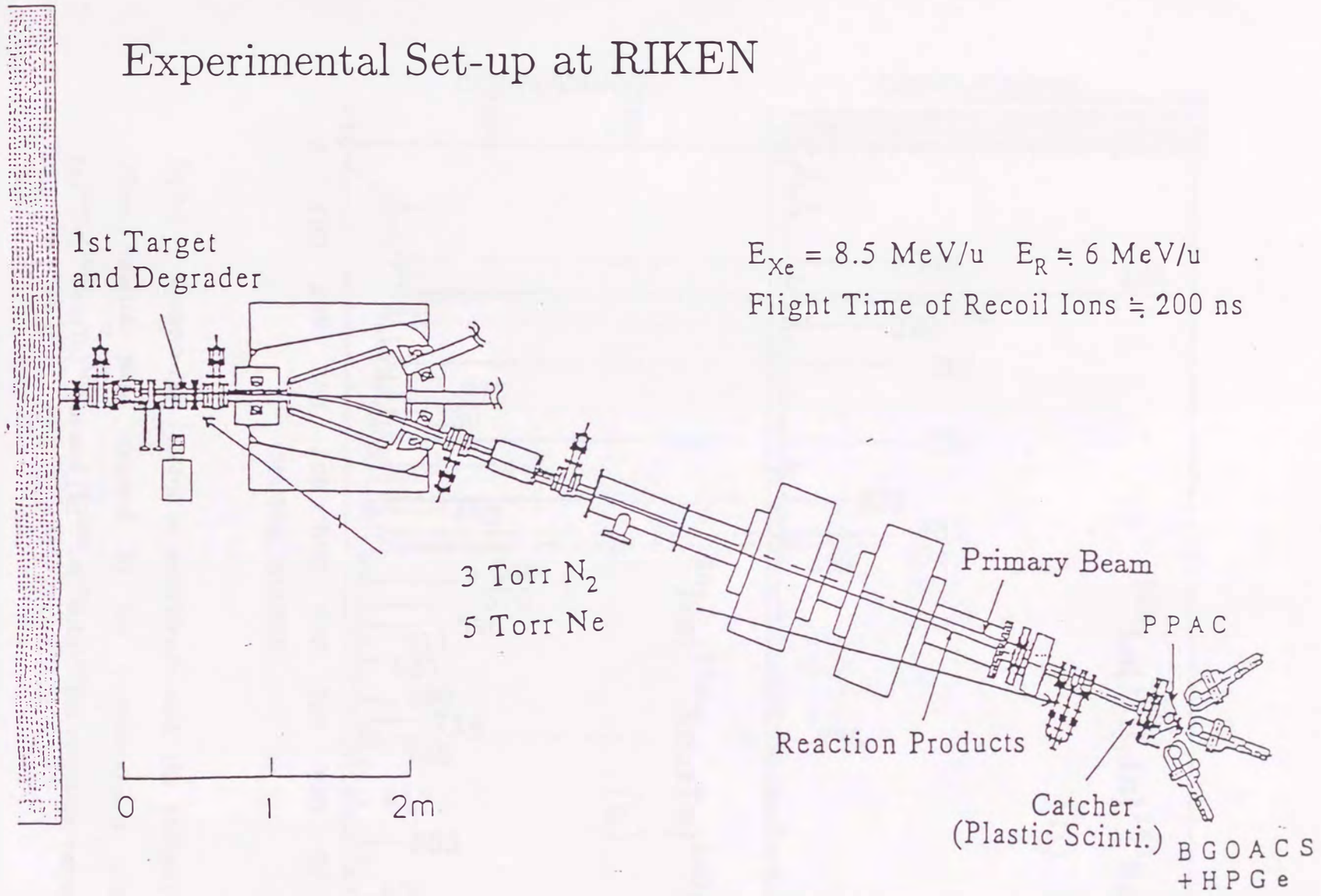

fig.2-1 A gas filled recoil ion separator of RIKEN.

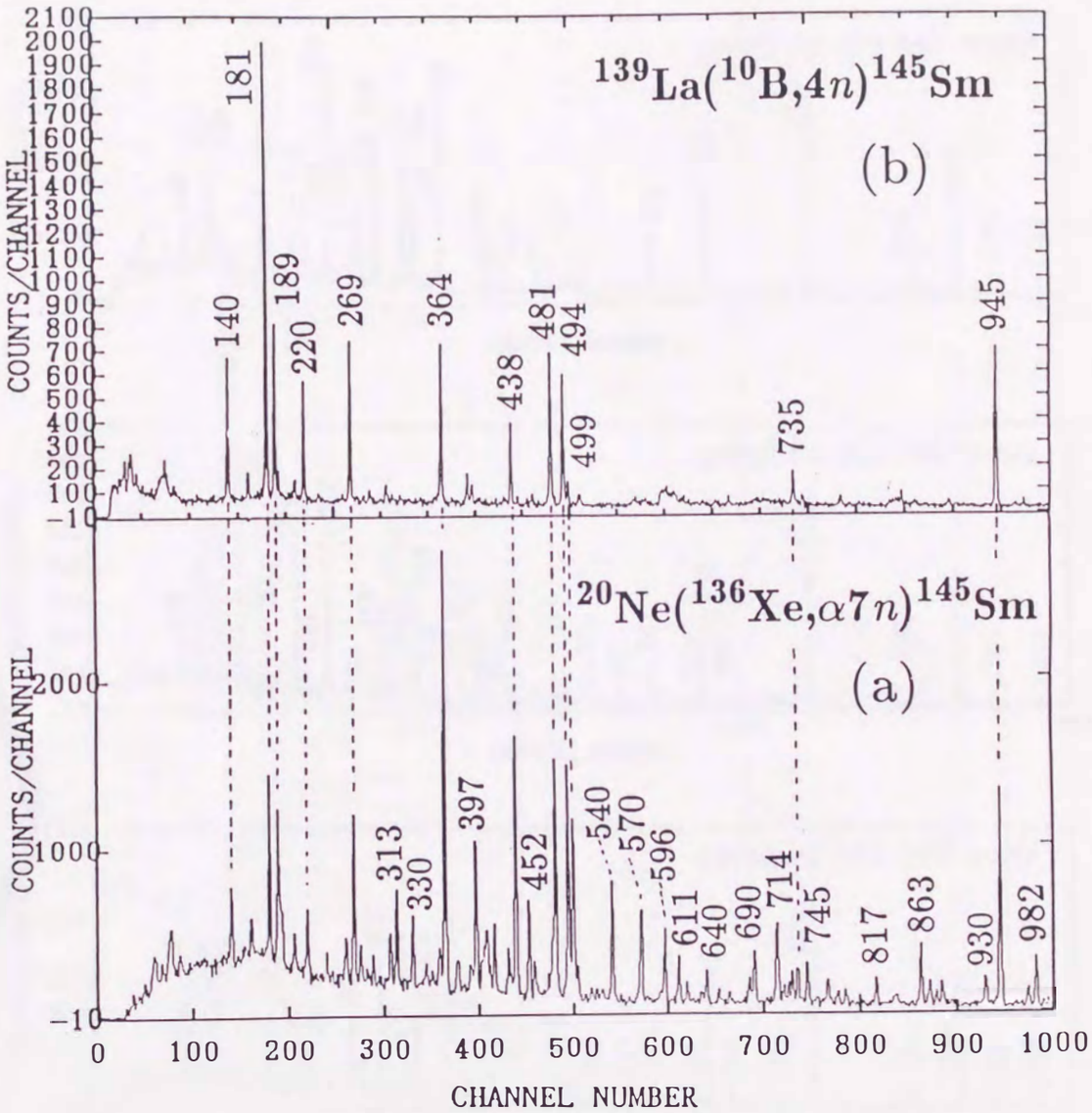

fig.2-2 Gamma-ray spectra in coincidence with the 1105keV γ-ray. These spectra were obtained by the $\gamma\gamma$-coincidences using the (a)^{20}Ne(^{136}Xe,α7n)^{145}Sm and (b)^{139}La(^{10}B,4n)^{145}Sm reactions, respectively.

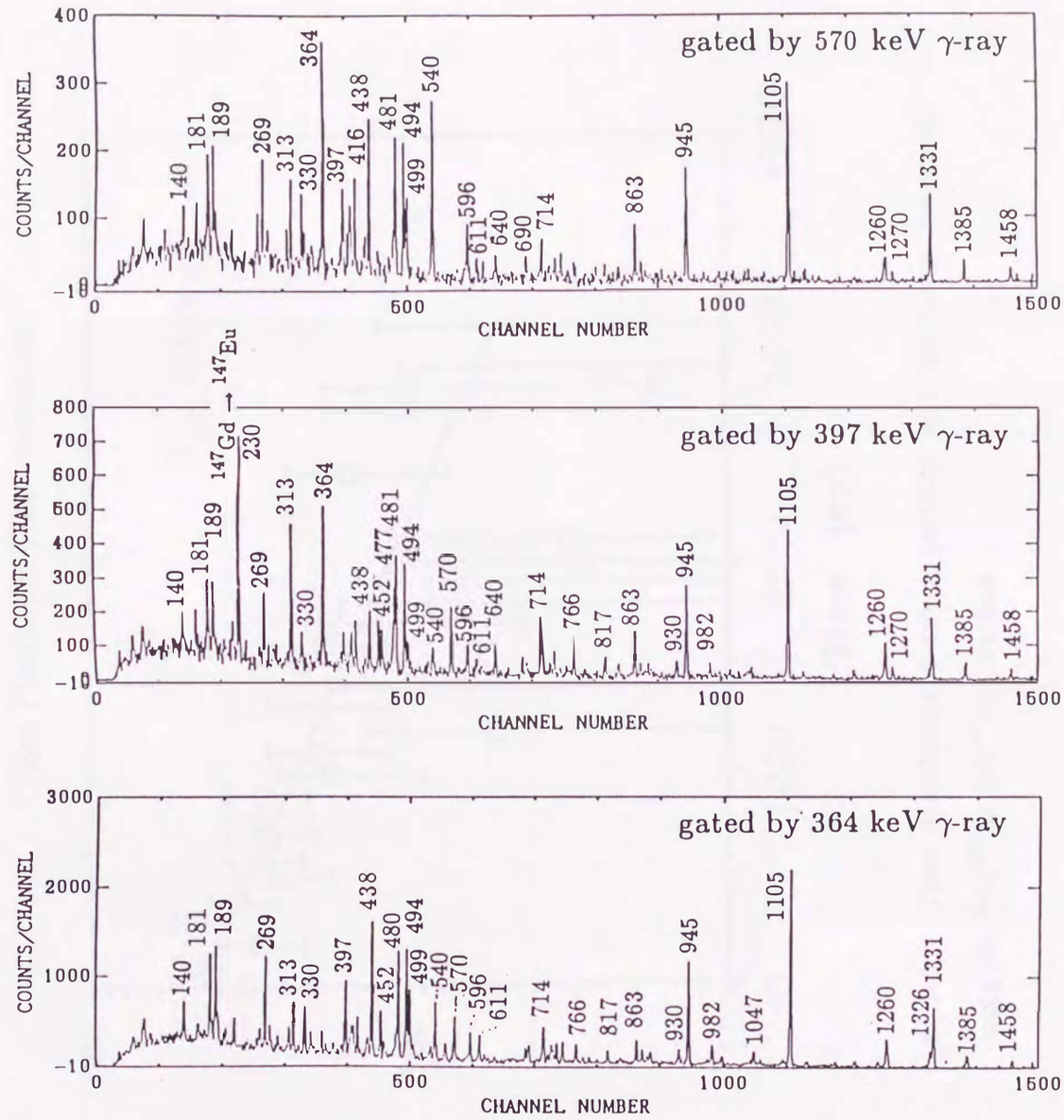

fig.2-3 Gamma-ray spectra gated by the 570, 397 and 364 keV γ-rays appeared in the ^{20}Ne(^{136}Xe,α7n)^{145}Sm reaction.

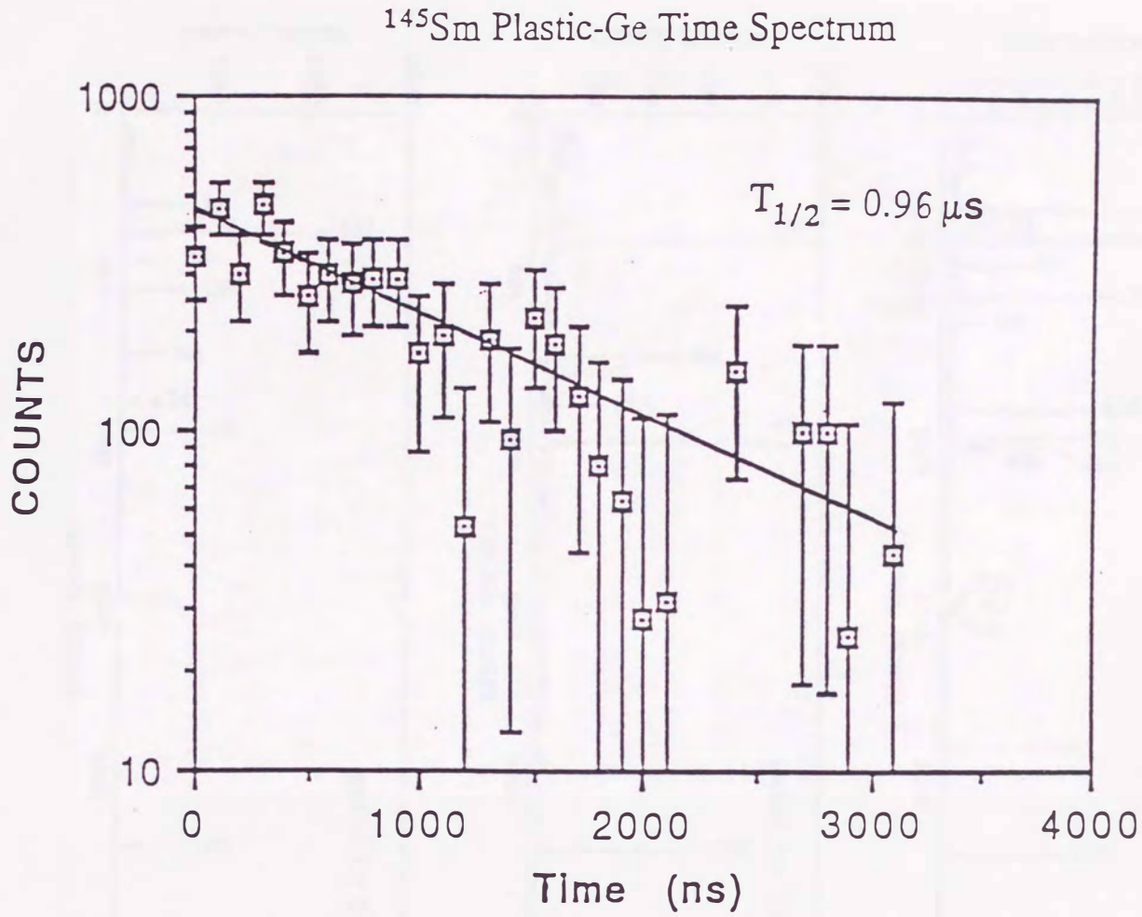

fig.2-4 Time distribution between particles and the γ-rays measured using the $^{16}O(^{136}Xe,7n)^{145}Sm$ reaction.

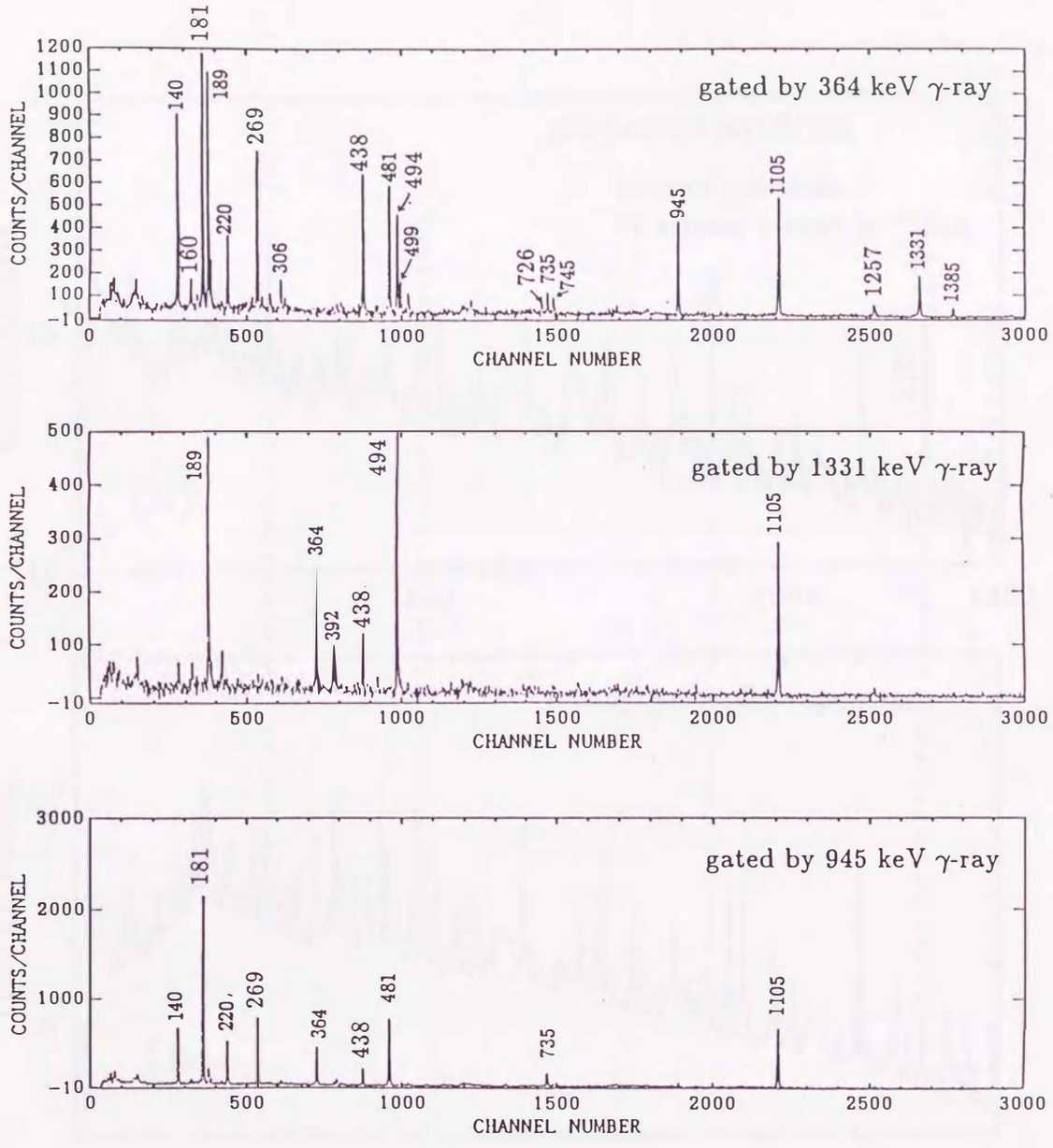

fig.2-5 Gamma-ray spectra gated by the 364, 1331 and 945 keV γ-rays obtained in the $^{139}La(^{10}B,4n)^{145}Sm$ reaction.

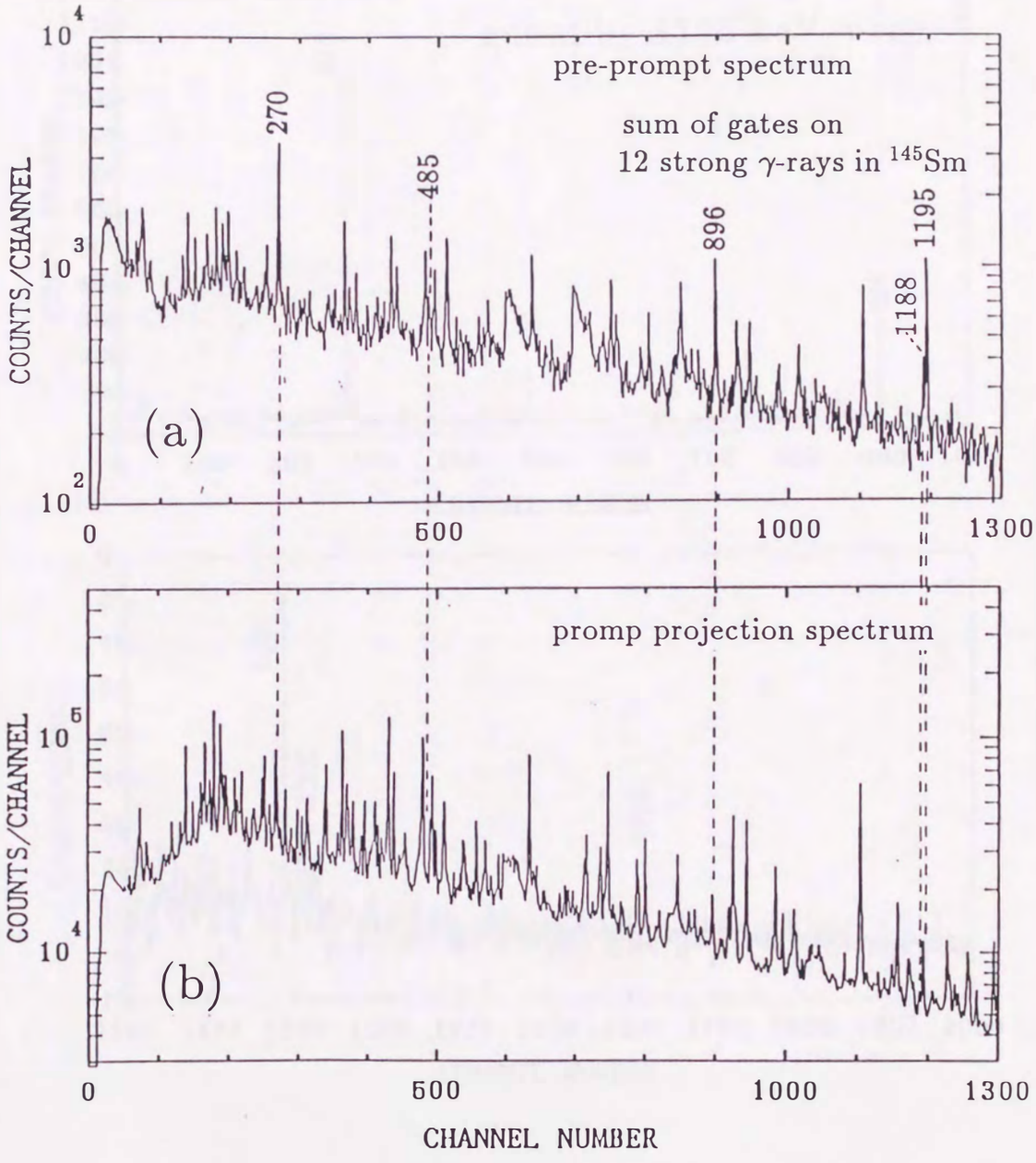

fig.2-6 In-beam γ-ray spectra taken by using the $^{138}Ba(^{13}C,6n)^{145}Sm$ reaction. (a)Pre-prompt spectrum summed for 12 strong γ-ray gated spectra of ^{145}Sm, and (b)projection spectrum obtained as a prompt $\gamma\gamma$-coincidences.

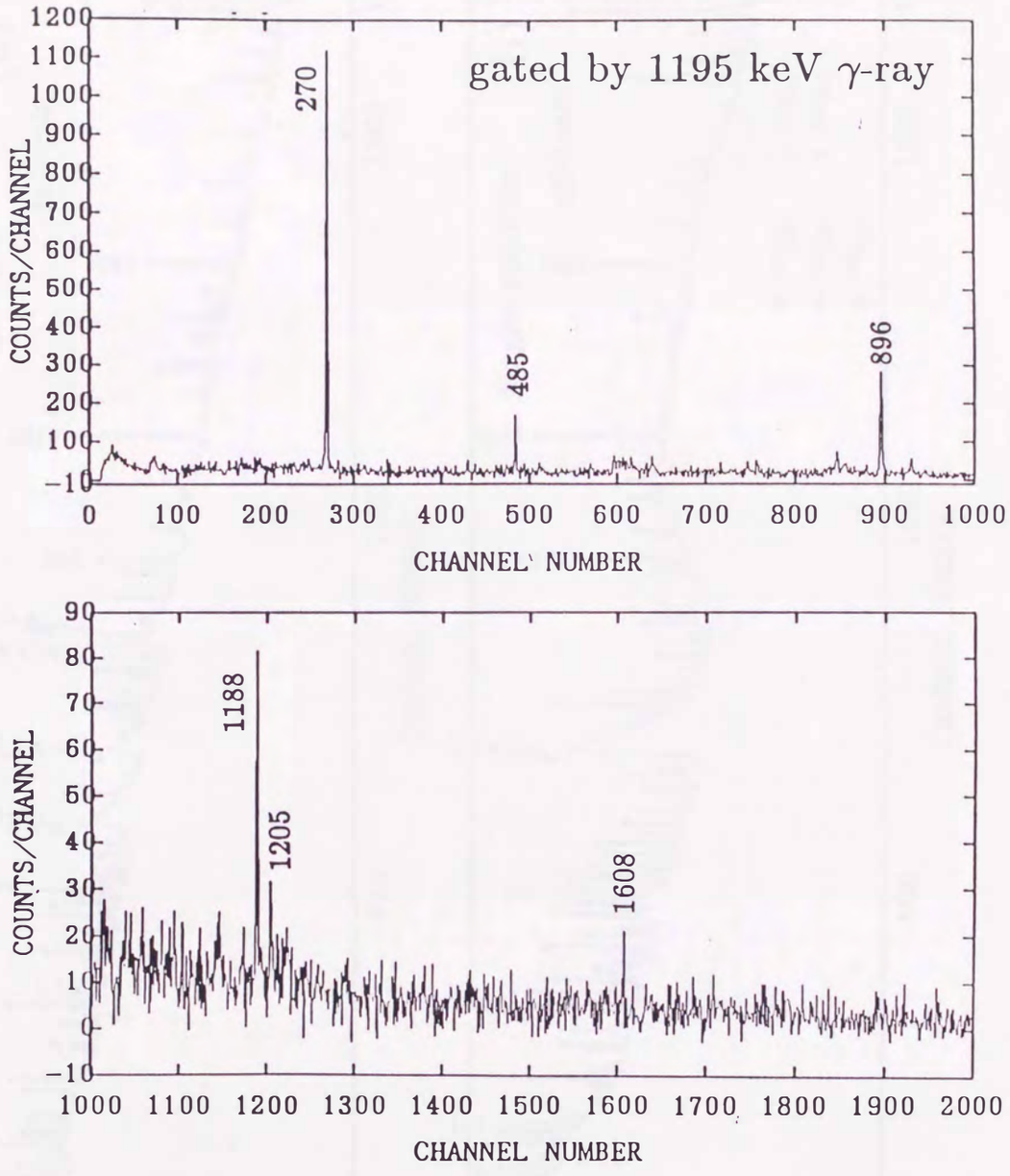

fig.2-7 Gamma-ray spectrum gated by the 1195 keV transition above the 0.96 μsec high-spin isomer in ^{145}Sm.

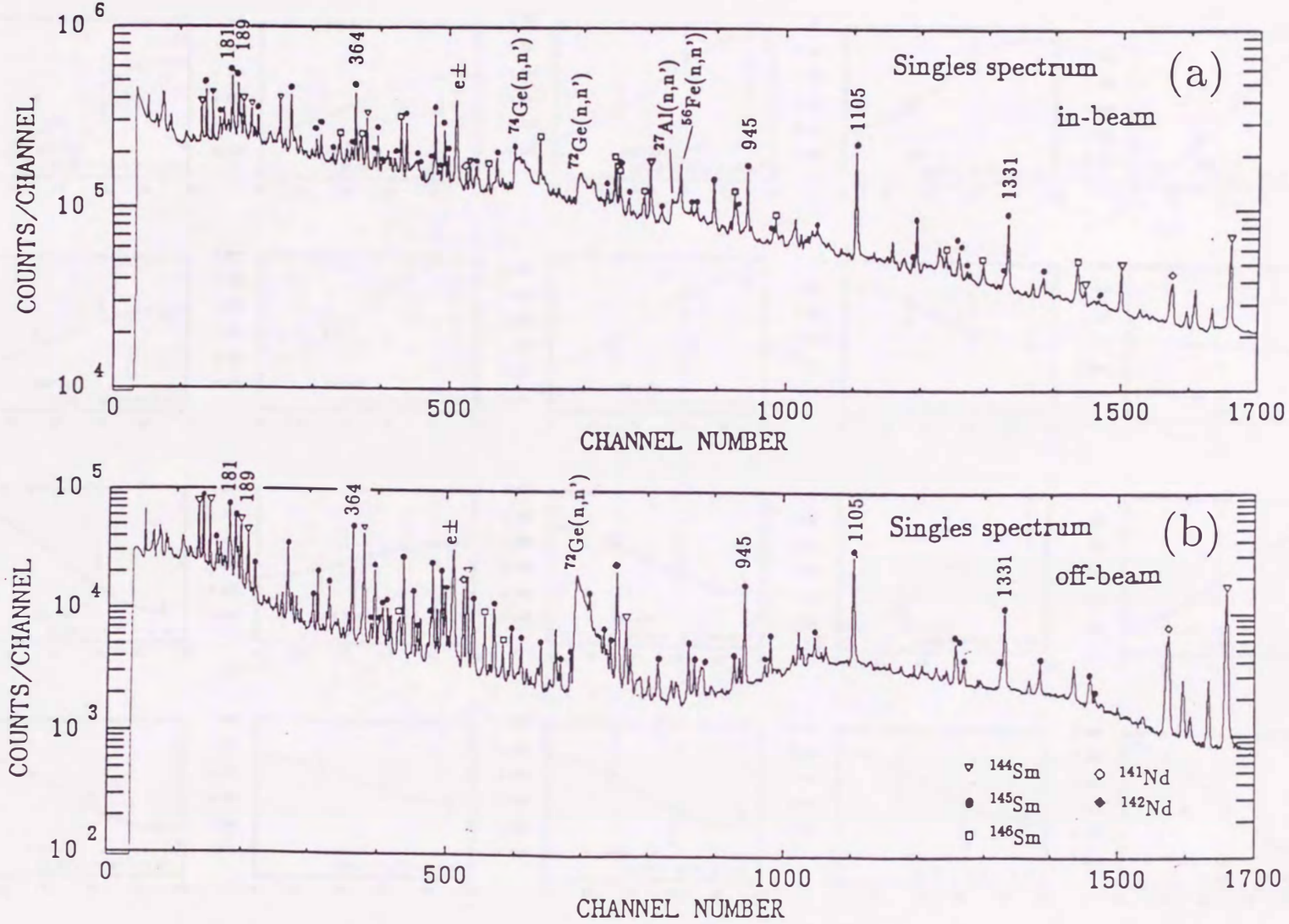

fig.2-8 Gamma-ray singles spectra taken for (a)an in-beam and (b)an off- beam region of the time spectrum of the $^{138}Ba(^{13}C,6n)^{145}Sm$ reaction with a pulsed beam.

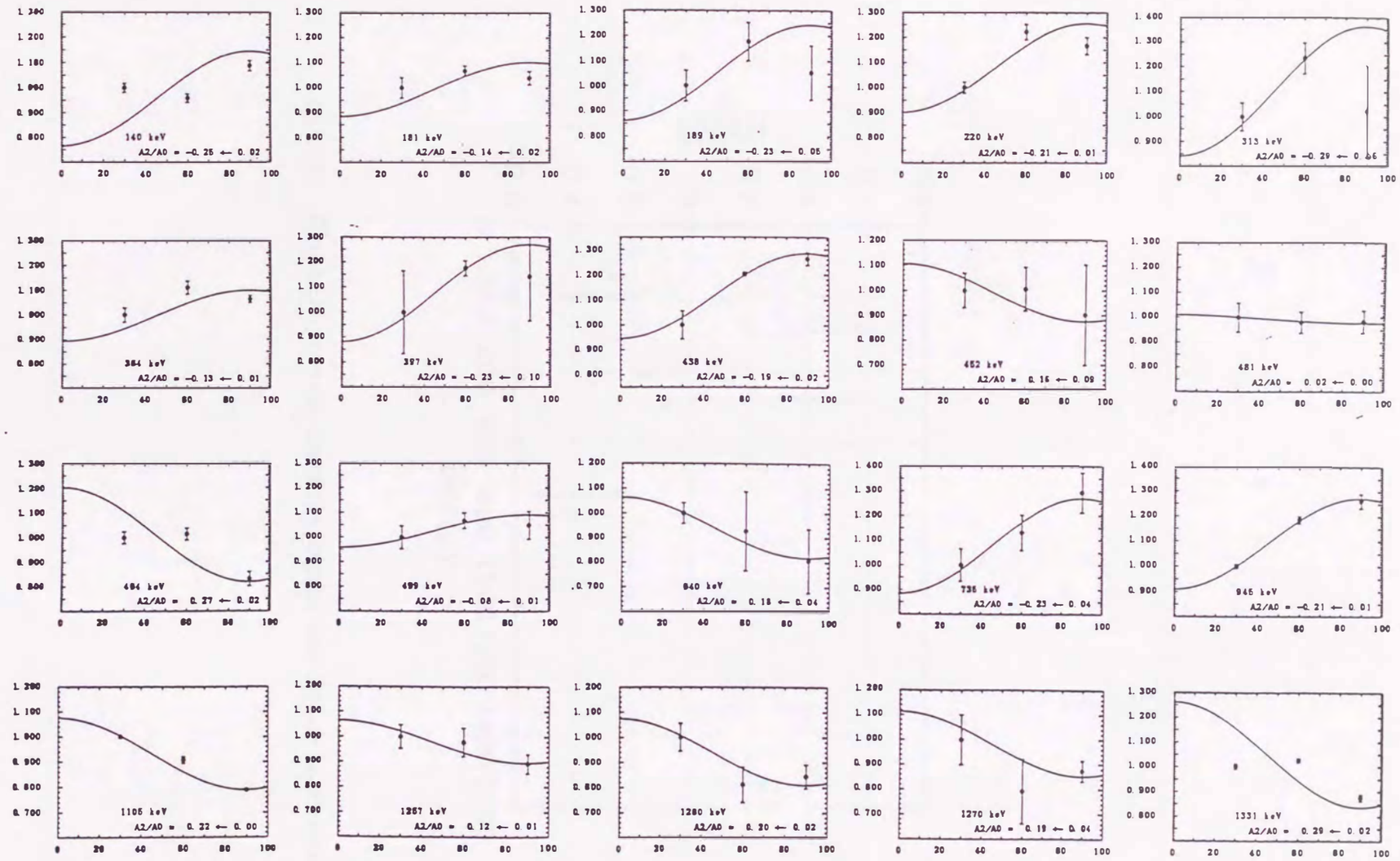

fig.2-9 Angular distributions fitted to eq.(1) obtained from the data taken by using the ^{138}Ba(^{13}C,6n)^{145}Sm reaction with pulsed beam.

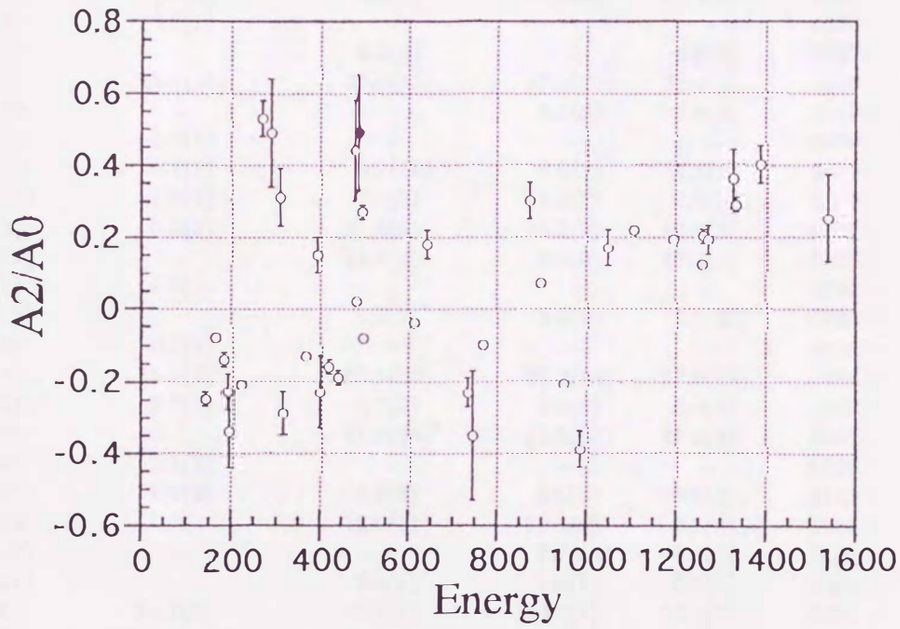

fig.2-10 Graphical presentation of the angular distribution coefficients.

Table 2-1 Intensities and placements in the level scheme of γ-rays observed in $\gamma\gamma$-coincidence measurements using different reactions.

γ-ray Energy [keV]	Intensity				E_i [keV]	→	E_f [keV]
	$^{139}La(^{10}B,4n)$	$^{20}Ne(^{136}Xe,\alpha 7n)$	$^{138}Ba(^{13}C,6n)$ Beam-on	$^{138}Ba(^{13}C,6n)$ Beam-off			
140.2(3)*	8.3(2)*	25.9(19)*	19.6(13)*	33.4(62)*	3120	→	2980
161.2(11)	2.4(3)	-	-	-	3483	→	3322
161.6(7)	-	5.5(4)	10.7(5)	15.0(6)*	5030	→	4869
171.7(5)	5.7(9)	-	-	-	4093	→	3922
180.5(5)	26.4(2)	34.3(9)	41.8(7)	46.2(6)	2231	→	2050
189.3(3)	10.5(1)	27.7(8)	37.0(24)	37.3(10)	3120	→	2930
191.2(15)	0.4(2)	4.4(6)	12.6(19)	7.2(5)	4421	→	4229
210.0(8)	1.5(1)	-	-	-	3140	→	2930
219.3(3)	-	-	-	-	3032	→	2811
219.8(3)	6.7(2)	9.6(4)	16.0(4)	12.4(8)	2930	→	2711
235.5(8)	0.7(1)	-	-	-	3376	→	3140
260.4(2)	-	6.1(3)	-	6.8(6)	6217	→	5957
268.6(3)	15.4(15)	25.0(13)	32.6(10)	31.4(2)	2980	→	2711
275.7(2)	-	-	8.1(5)	7.8(2)	5957	→	5681
282.1(5)	0.7(1)	-	-	-	4869	→	4587
289.0(5)	0.7(1)	9.1(10)	3.6(3)	4.1(5)	5030	→	4741
306.3(15)	1.9(2)	7.1(3)	12.6(7)	7.2(2)	4229	→	3922
313.3(2)	0.5(2)	21.6(5)	18.3(9)	16.2(3)	6217	→	5904
330.1(10)	-	14.7(4)	6.9(6)	13.2(2)	7675	→	7346
336.6(5)	0.9(1)	-	-	-	4791	→	4454
358.8(2)*	-	5.5(7)*	3.4(9)	5.5(37)*	6720	→	6362
360.7(5)	0.5(1)	-	-	-	4454	→	4093
364.1(5)	15.5(2)	60.9(86)	61.0(14)	57.0(14)	3484	→	3120
391.6(4)	3.7(3)	4.7(3)	8.4(5)	3.4(3)	3322	→	2930
396.5(2)	-	31.6(25)*	24.4(6)	27.2(4)	5904	→	5507
396.7(8)	2.1(2)	-	-	-	3376	→	2980
402.9(7)	1.1(2)	4.9(7)	6.5(8)	5.0(3)	6123	→	5720
408.1(13)	-	12.0(11)	10.4(8)	9.6(5)	7581	→	7173
415.5(10)	-	-	9.7(13)	9.1(3)	7346	→	6931
433.9(11)	-	6.8(4)	7.6(7)	7.7(6)	5681	→	5248
438.3(5)	14.2(7)	46.7(5)	40.3(3)	36.1(5)	3922	→	3484
452.3(8)	-	19.0(4)	6.9(6)	15.8(3)	7173	→	6720
452.8(20)	-	-	-	-	6669	→	6217
458.0(2)	-	6.1(2)	4.5(4)	5.3(2)	6362	→	5904
477.1(5)	0.8(4)	16.9(9)	14.3(25)	7.8(10)	5507	→	5030
480.5(5)	25.6(10)	39.7(10)	37.1(24)*	35.5(16)	2711	→	2231
493.6(5)	20.3(5)	42.5(15)	39.7(9)	31.2(13)	2930	→	2436
499.0(5)**	2.0(1)	24.5(12)	17.2(5)	17.6(5)	4421	→	3922
	-	-	-	-	6217	→	5720
503.3(10)**	-	8.3(15)	2.6(3)	2.6(3)	7675	→	7173
					6720	→	6217
512.4(3)	-	-	-	-	2050	→	1538
531.3(20)	-	-	-	-	7199	→	6669
539.9(10)	-	21.0(11)	16.8(8)	17.0(4)	8786	→	8246
570.3(10)	-	15.9(5)	7.4(10)	10.9(5)	8246	→	7675
595.6(10)	-	13.5(7)	12.4(36)*	16.0(57)*	7675	→	7080

Table 2-1 (continued)

γ-ray Energy [keV]	Intensity				E_i [keV]	→	E_f [keV]
	$^{139}La(^{10}B,4n)$	$^{20}Ne(^{136}Xe,\alpha 7n)$	$^{138}Ba(^{13}C,6n)$ Beam-on	Beam-off			
610.6(2)	1.9(3)	13.5(12)	5.7(13)	7.0(4)	5032	→	4421
639.9(7)	1.8(3)	5.3(20)	6.3(11)	7.3(4)	5030	→	4390
669.2(5)	1.7(3)	-	-	-	2890	→	2231
684.6(5)	-	15.1(7)	5.2(5)	5.8(7)	8786	→	8102
690.0(7)*	-	10.1(5)	12.5(73)*	4.8(21)*	5720	→	5030
713.6(10)	-	28.3(29)	7.5(41)	14.2(8)	6931	→	6217
725.8(5)	1.0(2)	7.6(4)	4.0(5)	3.0(7)	4648	→	3922
729.6(6)	-	4.9(3)	3.5(5)	4.2(7)	7902	→	7173
734.8(5)	8.0(5)	19.3(5)	9.3(6)	5.9(8)	2965	→	2231
744.6(15)	1.7(2)	7.2(4)	4.9(4)	6.7(9)	4229	→	3484
766.1(5)	-	12.4(6)	7.1(2)	4.3(4)	5507	→	4741
816.9(3)	-	4.7(3)	7.5(3)	5.1(31)*	6720	→	5904
862.6(10)	-	14.5(3)	5.8(4)	8.8(3)	7080	→	6217
871.7(2)	-	7.0(3)	10.0(5)	4.6(2)	5904	→	5032
884.8(6)	-	5.6(4)	6.2(18)	4.8(3)	8786	→	7902
929.7(5)	-	17.8(5)	6.9(19)*	5.9(7)	8102	→	7173
945.0(3)	43.3(6)	48.7(4)	49.3(6)	42.3(6)	2050	→	1105
973.6(5)	1.6(3)	7.3(5)	2.5(3)	3.2(5)	4093	→	3120
982.1(10)	-	4.3(3)	5.8(6)	10.5(6)	7199	→	6217
1013.5(9)*	0.4(2)*	-	-	-	4390	→	3376
1047.4(10)	-	13.7(33)	5.0(3)	9.1(8)	8246	→	7199
1066.6(17)	1.9(2)	-	-	-	4390	→	3322
1105.0(3)**	100.0(25)	100.0(9)	100.0(15)	100.0(19)	1105	→	0
	-	-	-	-	5030	→	3922
1207.0(13)	-	3.4(1)	1.6(7)	2.1(7)	8786	→	7581
1257.2(5)	2.7(5)	14.1(7)	11.5(7)	11.9(5)	4741	→	3484
1259.9(11)	1.1(3)	6.2(4)	5.7(5)	6.2(4)	5681	→	4421
1270.1(7)	2.2(2)	5.7(3)	3.7(6)	5.1(5)	4390	→	3120
1326.1(11)	2.2(4)	7.3(2)	4.1(4)	4.3(4)	5248	→	3922
1331.4(5)	35.7(6)	39.0(4)	40.4(4)	35.4(7)	2436	→	1105
1385.0(7)	1.2(2)	8.3(2)	8.4(5)	7.2(6)	4869	→	3484
1458.0(7)	-	7.8(2)	0.7(4)	4.1(2)	7675	→	6217
1467.5(5)	0.8(3)	-	-	-	4587	→	3120
1537.9(3)	9.0(3)	1.9(1)	1.6(3)	2.1(5)	1538	→	0
1705.5(3)	2.5(2)	7.5(2)	4.8(3)	8.2(3)	2811	→	1105

*Energy or intensity taken from coincidence spectra.

**Unresolved doublet.

Table 2-2 Intensities and placements in the level scheme of transitions above the 0.96 μsec high-spin isomer in ^{145}Sm. The data taken from in-beam $\gamma\gamma$-coincidnce measurement using the ^{138}Ba(^{13}C,6n)^{145}Sm reaction with pulsed beam.

γ-ray Energy [keV]	Intensity	E_i [keV]	→	E_f [keV]
270.3*	26.3(20)*	10251	→	9981
485.3*	4.0(10)*	12821	→	12335
515.9*	-	14560	→	14044
640.5*	-	12719	→	12078
879.8*	-	12335	→	11456
896.3*	-	11148	→	10251
930.6*	5.1(18)*	12078	→	11148
1187.7*	10.4(18)	12335	→	11148
1194.5*	29.3(6)	9981	→	8786
1204.7	-	11456	→	10251
1223.9	-	14044	→	12821
1607.8	-	14428	→	12821

*Energy or intensity taken from coincidence spectra.
The energies are determined with the experimental accuracy of ±0.5keV.

Table 2-3(a) Summary of γ-ray angular distribution data taken from in-beam spectrum using the ^{138}Ba(^{13}C,6n) reaction with pulsed beam.
(a)List of transitions under 0.96 μsec high-spin isomer.

γ-ray Energy [keV]	Angular Distribution A2/A0	ΔI	tentative Assignment I_i	→	I_f
140.2(3)*	-0.25(2)	1	23/2+	→	21/2+
161.2(11)	-	-	25/2+	→	(21/2)
161.6(7)	-0.08(1)	1	(31/2)	→	(29/2)
171.7(5)	-	-	(25/2)	→	27/2+
180.5(5)	-0.14(2)	1	17/2−	→	15/2−
189.3(3)	-0.23(5)	1	23/2+	→	21/2+
191.2(15)	-0.34(10)	1	29/2+	→	(27/2)
210.0(8)	-	-	-	→	21/2+
219.3(3)	-	-	-	→	(15/2)
219.8(3)	-0.21(1)	1	21/2+	→	19/2−
235.5(8)	-	-	-	→	-
260.4(2)	-	-	(37/2)	→	-
268.6(3)	-	-	21/2+	→	19/2−
275.7(2)	-	-	-	→	(33/2)
282.1(5)	-	-	(29/2)	→	-
289.0(5)	0.49(15)	1	(31/2)	→	(29/2)
306.3(15)	0.31(8)	0	(27/2)	→	27/2+
313.3(2)	-0.29(6)	1	(37/2)	→	(35/2)
330.1(10)	-	1	(43/2)	→	(41/2)
336.6(5)	-	-	-	→	-
358.8(2)*	0.65(21)	1	(39/2)	→	(37/2)
360.7(5)	-		-	→	(25/2)
364.1(5)	-0.13(1)	1	25/2+	→	23/2+
391.6(4)	0.15(5)	0	(21/2)	→	21/2+
396.5(2)	-0.23(10)	1	(35/2)	→	(33/2)
396.7(8)	-	-	-	→	21/2+
402.9(7)	0.53(79)	-	-	→	-
408.1(13)	-	-	(47/2)	→	(43/2)
415.5(10)	-0.16(2)	1	(41/2)	→	(39/2)
433.9(11)	-	-	(33/2)	→	(31/2)
438.3(5)	-0.19(2)	1	27/2+	→	25/2+
452.3(8)	0.16(9)	2	(43/2)	→	(39/2)
452.8(20)	-	-	-	→	(37/2)
458.0(2)	-0.28(8)	1	(37/2)	→	(35/2)
477.1(5)	0.44(14)	1	(33/2)	→	(31/2)
480.5(5)	0.023(3)	1	19/2−	→	17/2−
493.6(5)	0.27(2)	2	21/2+	→	17/2+
499.0(5)**	-0.08(1)	1	29/2+	→	27/2+
	-	-	(37/2)	→	-
503.3(10)**	0.31(18)	1	(39/2)	→	(37/2)
	-	-	(43/2)	→	(43/2)
512.4(3)	-	-	15/2−	→	(11/2−)
531.3(20)	-	-	(43/2)	→	-
539.9(10)	-	-	(49/2+)	→	(47/2)
570.3(10)	-	-	(47/2)	→	(43/2)
595.6(10)	-	-	(43/2)	→	(41/2)

Table 2-3(a) (Continued)

γ-ray Energy [keV]	Angular Distribution A2/A0	ΔI	tentative Assignment I_i	→	I_f
610.6(2)	-0.04(1)	1	(31/2)	→	29/2+
639.9(7)	0.18(4)	2	(31/2)	→	(27/2)
669.2(5)	-	-	-	→	17/2−
684.6(5)	-	-	(49/2+)	→	(47/2)
690.0(7)*	-	-	-	→	(31/2)
713.6(10)	-0.42(12)	1	(39/2)	→	(37/2)
725.8(5)	-	-	-	→	27/2+
729.6(6)	-	-	(47/2)	→	(43/2)
734.8(5)	-0.23(4)	1	19/2(+)	→	17/2−
744.6(15)	-0.35(18)	1	(27/2)	→	25/2+
766.1(5)	-0.10(1)	2	(33/2)	→	(29/2)
816.9(3)	-0.08(1)	2	(39/2)	→	(35/2)
862.6(10)	-	-	(41/2)	→	(37/2)
871.7(2)	0.30(5)	2	(35/2)	→	(31/2)
884.8(6)	-	-	(49/2+)	→	(47/2)
929.7(5)	-0.25(4)	2	(47/2)	→	(43/2)
945.0(3)	-0.21(1)	1	15/2+	→	13/2−
973.6(5)	-0.49(20)	1	(25/2)	→	23/2+
982.1(10)	-	-	(43/2)	→	(37/2)
1013.5(9)*	-	-	(27/2)	→	-
1047.4(10)	0.17(5)	2	(47/2)	→	(43/2)
1066.6(17)	-	-	(27/2)	→	-
1105.0(3)**	0.215(2)	3	13/2+	→	7/2−
	-	-	(31/2)	→	27/2+
1207.0(13)	-	-	(49/2+)	→	(47/2)
1257.2(5)	0.12(1)	2	(29/2)	→	25/2+
1259.9(11)	0.20(2)	2	(33/2)	→	29/2+
1270.1(7)	0.19(4)	2	(27/2)	→	23/2+
1326.1(11)	0.36(8)	2	(31/2)	→	27/2+
1331.4(5)	0.29(2)	2	17/2+	→	13/2+
1385.0(7)	0.40(5)	2	(29/2)	→	25/2+
1458.0(7)	1.05(59)	3	(43/2)	→	(37/2)
1467.5(5)	-	-	-	→	23/2+
1537.9(3)	0.25(12)	2	(11/2−)	→	7/2−
1705.5(3)	-0.18(9)	1	(15/2)	→	13/2+

*Energy taken from coincidence spectra.
**Unresolved doublet.

Table 2-3(b) List of transitions above the high-spin isomer.

γ-ray Energy [keV]	Angular Distribution A2/A0	ΔI	tentative Assignment I_i	→	I_f
270.3*	0.53(5)	1	(55/2)	→	(53/2)
485.3*	0.49(16)	2	(61/2)	→	(59/2)
515.9*	-	-	(65/2)	→	(63/2)
640.5*	-	-	-		
879.8*	-	-	(59/2)	→	-
896.3*	0.073(3)	1	(57/2)	→	(55/2)
930.6*	-	-	-	→	(57/2)
1187.7*	−0.95(26)	1	(59/2)	→	(57/2)
1194.5*	0.19(1)	2	(53/2)	→	($49/2^+$)
1204.7	-	-	-	→	(55/2)
1223.9	-	-	(63/2)	→	(61/2)
1607.8	-	-	-	→	(61/2)

*Energy taken from coincidence spectra.

3. Construction of Level Scheme

3-1 Low-Lying States

A level scheme of ^{145}Sm was previously reported up to the $29/2^+$ state at 4.4 MeV[26]. In this work, the low-lying level scheme was constructed based on the $\gamma\gamma$-coincidence data taken by using the ^{139}La(^{10}B,4n)^{145}Sm reaction at Kyushu University. This level scheme includes 27 new γ-rays as is shown in fig.3-1.

A γ-ray of 1105 keV was known to be a transition between the $13/2^+$ and $7/2^-$ states. However, a γ-ray of the same energy was observed in the γ-ray spectrum gated by itself. This γ-ray peak must be a doublet. The second one is tentatively placed between the 3922 and 5030 levels. An unobserved low-energy transition between the 2980 and 2965 keV states is suggested by the γ-ray coincidence relations of the 140 and 735 keV γ-rays. This transition could not be observed in this work, because the transition energy was too low to detect. The same occurs between the 2980 and 2930 keV levels. A 50 keV transition must be exist because the 140 and 494 keV γ-rays are in coincidence. The ordering of each levels was determined considering the intensity balances and the coincidence relations.

3-2 High-Spin States

A decay scheme of the high-spin isomer in ^{145}Sm was constructed based on the $\gamma\gamma$-coincidence data taken by using the ^{20}Ne(^{136}Xe,α7n)^{145}Sm reaction. Figure 3-2 shows the resulted decay scheme. Two data obtained by using different reactions were able to establish this complex decay scheme. The ordering of each level was determined by the coincidence relations and γ-ray intensities. In the

decay scheme of this isomer in ^{145}Sm, 54 new γ-rays and 36 new levels were introduced. The excitation energy of the high-spin isomer in ^{145}Sm was determined to be 8.8 MeV.

Twelve transitions and 11 levels were newly identified above the isomer. The preprompt and prompt $\gamma\gamma$-coincidence spectra, as shown in fig.2-6 and fig.2-7, are obtained in the experiment made by using the ^{138}Ba(^{13}C,6n)^{145}Sm reaction. A level scheme was extended up to the state at 14.6 MeV above the high-spin isomer based on the coincidence relations and γ-ray intensities. Including the information obtained by three different experiments, the proposed level scheme is displayed in fig.3-2. The diagram to the right of this figure shows the intensity of the feeding γ-rays at each level.

Spin and parity of each level up to the $29/2^+$ state at 4.4 MeV was previously assigned from angular distribution and conversion electron measurements[26]. In this work, multipolarities of transitions were determined based on the γ-ray angular distributions taken by using the pulsed beam of ^{13}C at JAERI. Angular distribution coefficients, A_2/A_0, are listed in Table 2-3. Their graphical presentation is given in fig.2-10. The pure stretched E2 and M1 values are considered to be $0.1 \sim 0.3$ and -0.1, respectively. Any other values were considered to result from the mixing of E2 and M1. The spin change, ΔI, of each transition was deduced based on this assumption. The tentative spin assignment of each level was given by using both of ΔI values and γ-ray cascade cross-over relations. However, transitions deexciting the levels in the region between the 6.0 and 8.8 MeV show the isotropic distribution. The spin value of the high-spin isomer was obtained to be $49/2^+$ based on DIPM calculation as discussed below (in section 4-1). Spin values in this energy region were proposed by γ-ray cascade relations and this assignment of $49/2^+$ isomer. The values of ΔI and spin assignments of transitions are listed in Table 2-3.

The 540, 685, 885 and 1207 keV transitions were identified in this work to

deexcite the high-spin isomer at 8.8 MeV. Total intensity of 4 γ-rays is 45% with respect to that of the 1105 keV γ-ray.

In the 4.4 $\sim$ 6.2 MeV energy region, the intensity balances of γ-rays between populating and depopulating the states do not hold. Many unobserved high-energy γ-rays seem to exist.

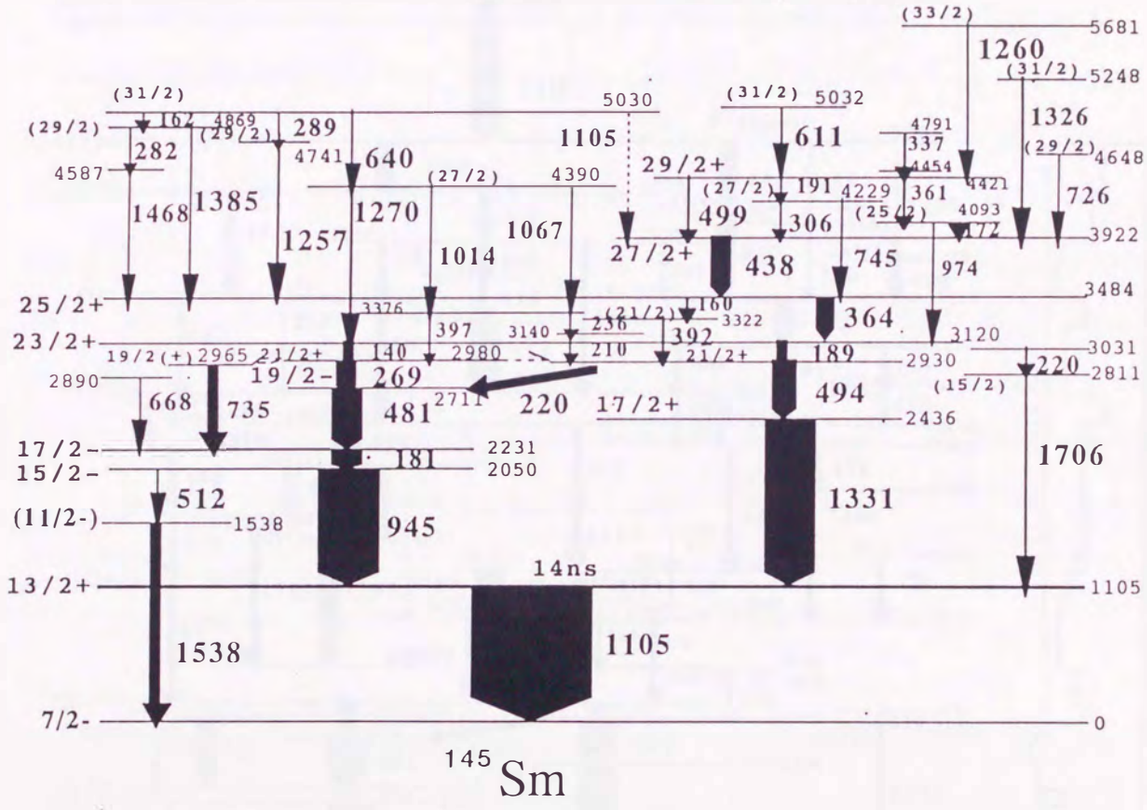

^{145}Sm

fig.3-1 Low-lying level scheme in ^{145}Sm as observed in the ^{139}La(^{10}B,4n)^{145}Sm reaction.

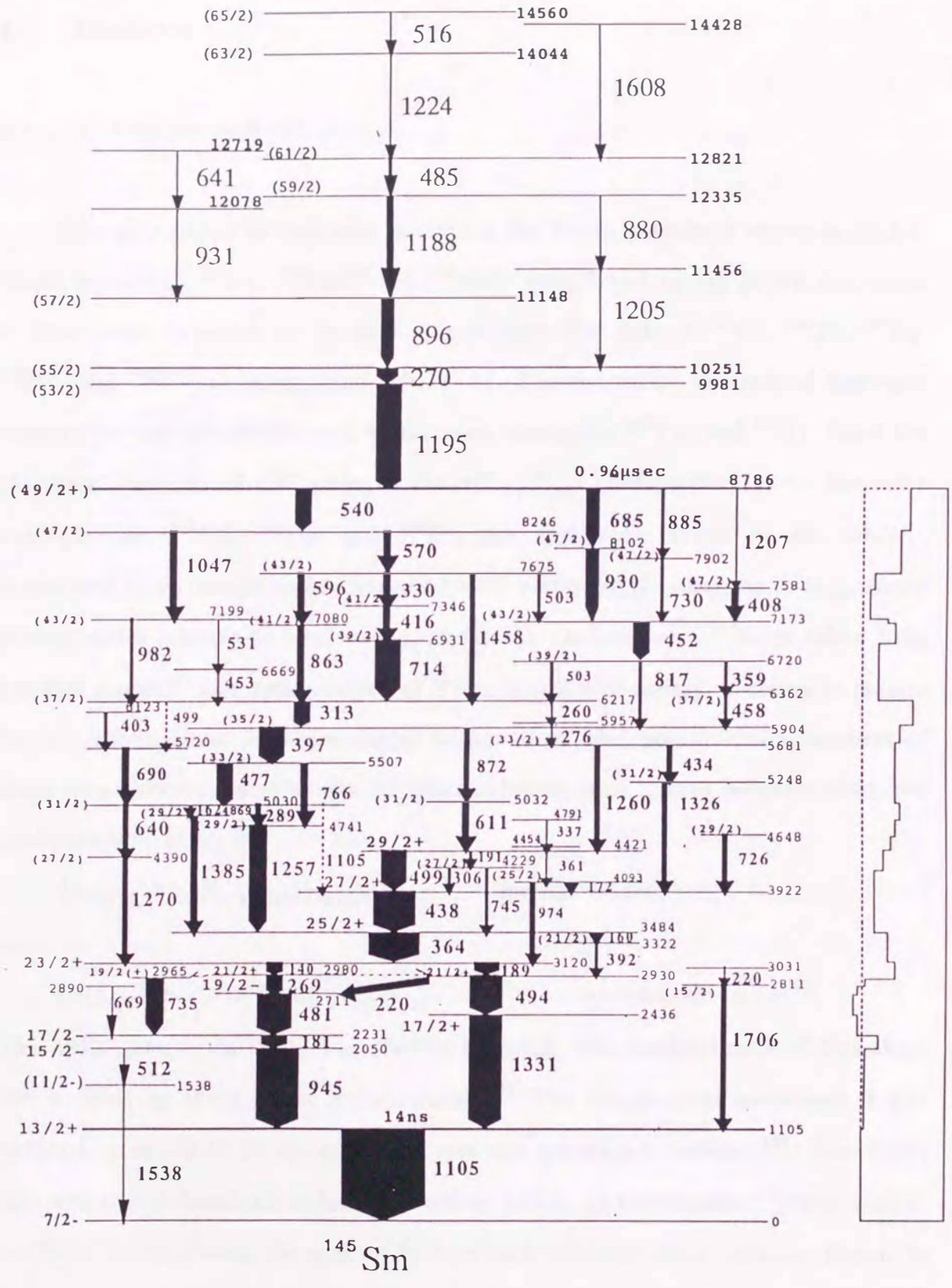

^{145}Sm

fig.3-2 Level scheme including 0.96 μsec high-spin isomer in ^{145}Sm. The diagram to the right displays the feeding intensities for each levels taken from the data using the ^{20}Ne(^{136}Xe,α7n)^{145}Sm reaction.

4. Discussion

4-1. Systematics of N=83 isotones

The systematics of high-spin isomers of the N=83 isotones is shown in fig.4-1. Three isomers in ^{145}Sm, ^{144}Pm[35] and ^{146}Eu[36] were found by our group in a series of experiment to search for the high-spin isomers. The data of ^{147}Gd, ^{148}Tb, ^{149}Dy, ^{150}Ho and ^{151}Er are taken from refs.37~41. The excitation energies of high-spin isomers decrease as proton number increases except for ^{144}Pm and ^{151}Er. Since the excitation energies of 10^+ state of the $\pi(h_{11/2}{}^2)_{10^+}$ configuration show the same tendency for ^{146}Gd, ^{148}Dy and ^{150}Er, the systematic trend of the isomers mentioned above seems to be caused at least partly by the energies of $h_{11/2}$ single proton states relative to neutron $f_{7/2}$ states. As the isomer of ^{151}Er is taken from the first report[41] and data analysis of ^{144}Pm is still preliminary, it seems to require further informations on these nuclei to pin down this points. Configurations of these isomers were found by the DIPM calculation to be almost uniquely stretched configurations of,

$\{\pi h_{11/2}{}^2\nu(f_{7/2}h_{9/2}i_{13/2})\}_{49/2^+}$: for odd nuclei[14]

and

$\{\pi(d_{5/2}{}^{-1}h_{11/2}{}^2)\nu(f_{7/2}h_{9/2}i_{13/2})\}_{27^+}$: for odd-odd nuclei[24].

The $49/2^+$ isomer in ^{147}Gd was studied in detail. The configuration of this state was verified by the g-factor measurements[17]. The deformation parameter β was deduced to be -0.19 by the measurements of a quadrupole moment[18]. Therefore, this isomer is determined to have the oblate shape. As the nucleus ^{145}Sm is similar to ^{147}Gd in excitation energies of isomers and complex decay scheme shown in fig.3-2 and 4-2, respectively, the high-spin isomer in ^{145}Sm may be expected to have the oblate shape and the same configuration as that of ^{147}Gd.

Systematics of the excited states of odd-A nuclei with N=83 is shown in

fig.4-3. The data of ^{145}Sm is obtained in this work, and those of ^{143}Nd, ^{147}Gd, ^{149}Dy and ^{151}Er are taken from refs.42), 37), 39) and 41). The spins and parities of the ground states in all nuclei are known to be $7/2^-$ of $\nu f_{7/2}$.

The $13/2^+$ states are isomers with nano seconds half lives in all cases. In the nuclei ^{145}Sm and ^{147}Gd, these states are fed through two branches with comparable intensities. The measured half lives indicate enhancements by about factors of 10 compared to the E3 Weisskoph estimates. The doubly-even core nuclei with N=82 have the 3^- octupole states, which deexcite by E3 transitions with enhancements of the same order. Systematics of level schemes of N=82 doubly-even isotones is shown in fig.4-4. The data of ^{142}Nd, ^{144}Sm ^{146}Gd, ^{148}Dy and ^{150}Er are taken from refs.43$\sim$ 47. Excitation energies of the 3^- states are the lowest in ^{146}Gd, and increase as the proton number increases and decreases from Z=64. The E3 transition from the 3^- state to the 0^+ ground state is known[45] to be enhanced by a factor of 37. The nucleus ^{146}Gd is interpreted to be doubly closed shell with N=82 and Z=64, because of first excited 3^- state[21] and the excitation energy of the lowest 2^+ state which is higher by 300 keV than those of other N=82 nuclei[22]. The $13/2^+$ states in N=83 isotones have the similar tendency of excitation energy and large E3 enhancement to the 3^- states in N=82 isotones. Therefore these states are considered to have a configuration of a single $f_{7/2}$ neutron coupled to the 3^- octupole core excitation.

Isomers of $27/2^-$ and 10^+ are observed in N=83 odd and N=82 doubly-even isotones, respectively, in the region of Z$\geq$64. These isomers with N=83 and 82 are assigned to be $\pi h_{11/2}{}^n \nu f_{7/2}$ and $\pi h_{11/2}{}^n$ aligned configurations, where n is the $\pi h_{11/2}$ occupation number[48]. However, the nuclei with Z<64 have no such isomers. In calculation for ^{145}Sm using a deformed independent particle model (shown in section 4-2), the $27/2^-$ state with $\pi h_{11/2}{}^2 \nu f_{7/2}$ structure appears at 4.45 MeV excitation energy as yrast state. However, corresponding state was not experimentally found.

4-2. Configuration assignment

The configurations of the low-lying high-spin states in ^{145}Sm were previously reported[26]. The odd-parity levels were interpreted as three-quasi particle states resulted from the coupling between the two proton hole excitations of ^{144}Sm and the $f_{7/2}$ valence neutron. The positive parity states up to the $25/2^+$ state at 3.48 MeV were considered to involve the proton particle-hole excitations with one proton in $h_{11/2}$.

The assignments of these configurations were made in the framework of the shell model[26] by using the empirical single-particle energies extracted from the data of neighbouring nuclei.

The above mentioned weak coupling picture was applied below to the (37/2) state at 6.22 MeV, since the excited states are known only up to the $16^{(+)}$ state in the core nucleus ^{144}Sm.

In the ^{144}Sm core, the states of the proton particle-hole excitations are known[44]. The proton one particle three hole (1p3h) excitation occurs in the energy region between the 4.7 and 5.7 MeV. This core excitation causes several parallel high-energy E2 transitions between the 1.3 and 1.5 MeV feeding the $\pi(h_{11/2}{g_{7/2}}^{-1})_{9-}$ state. The similar transitions are observed in ^{145}Sm above the $23/2^+$ and $25/2^+$ states with $\nu f_{7/2}$ coupled to the 8^- and 9^- of the $\pi(h_{11/2}{g_{7/2}}^{-1})$ configurations, respectively. Therefore, the configurations of the states of (27/2) at 4.39 MeV, (29/2) at 4.74 and at 4.87 MeV, (31/2) at 5.03 MeV and (33/2) at 5.51 MeV were assigned to be the $\nu f_{7/2}$ coupled to the 10^-, 11^-, 12^- and 13^- of the $\pi(h_{11/2}{g_{7/2}}^{-1}{d_{5/2}}^{-2})$ one particle three hole (1p3h) excitation, respectively. The (35/2) state may be understood to be of $\pi(h_{11/2}{g_{7/2}}^{-2}{d_{5/2}}^{-1})_{14-}\nu f_{7/2}$ configuration.

In ^{144}Sm, the proton two particle two hole (2p2h) core excitation appears above the state at 6.1 MeV. The (37/2) state in ^{145}Sm is interpreted to be $\pi({h_{11/2}}^2{g_{7/2}}^{-1}{d_{5/2}}^{-1})_{15+}\nu f_{7/2}$ configuration.

Above the (37/2) state, the experimental level scheme was compared with that of the DIPM calculation[23] and is displayed in fig.4-7. This model deals with independent particle configurations in an axially symmetric deformed potential. A single-particle energy was calculated using Woods-Saxon potential with an axially symmetric shape and single-particle orbits were given as a function of deformation. A pairing force was taken into account varying of the gap parameters after particle number projections. The relative spherical single-particle energies of levels of $1g_{7/2}$, $2d_{5/2}$, $1h_{11/2}$, $3s_{1/2}$ and $2d_{3/2}$ for proton and of $1h_{11/2}$, $3s_{1/2}$, $2f_{7/2}$, $1h_{9/2}$ and $i_{13/2}$ for neutron were extracted from experimental data. From the total of these single-particle energies of the orbits occupied by nucleons, Strutinsky's smooth sum is subtracted and replaced by the liquid drop energy. The sum of single-particle angular momenta along the symmetry axis is interpreted to correspond to a measured total angular momentum of the nucleus. The yrast state energies are taken from the minimum sum energy in the deformation space for each total angular momentum.

In fig.4-7, yrast states taken from both of the experiment (left side) and the DIPM calculation (right side) are shown. The E3 transition deexciting the $13/2^+$ state is enhanced by a factor of 30. Because of this collectivity, the experimental energy of this state is lower than the calculated pure $i_{13/2}$ single-particle energy. The yrast states taken from the calculation are compared with the experimental ones by the excitation energies relative to that of the $13/2^+$ state. The experimental and theoretical excitation energies of the $49/2^+$ levels are almost the same. Moreover, the experimental excitation energies of the other levels correspond well to those of the calculations. However, the levels including a single neutron $h_{9/2}$ were not observed. The $49/2^+$ state has $\pi h_{11/2}{}^2\nu(f_{7/2}h_{9/2}i_{13/2})$ configuration according to the DIPM calculation. As the yrast-state configurations below this state consist of one neutron and fore or six proton valence particles and holes, the transitions from the $49/2^+$ state are retarded to populate these levels originated

from the one or two particles configuration change. Then, this state becomes to be isomer. The isomer at 8.8 MeV is interpreted to corresponds to the $49/2^+$ state.

As described in section 4-1, the $27/2^-$ state with $\pi h_{11/2}{}^2 \nu f_{7/2}$ configuration appears as the yrast states from the DIPM calculation. However, the corresponding state was not observed in experiments. The configuration of the experimental yrast $27/2^+$ state at 4.1 MeV is assigned to be $\pi(h_{11/2}d_{5/2}{}^{-3})\nu f_{7/2}$, which appears in the non-yrast state by calculation. The yrast states up to the (39/2) state deduced by the experiments correspond to those of the calculation, based on the configuration assignment assuming a single neutron coupled to the ^{144}Sm core excitation, mentioned above. The experimental levels between the (41/2) and (47/2) are corresponded to calculated yrast states with the same spin.

Above the $49/2^+$ state, experimental yrast states seem to originate from three configurations, shown in fig.4-6. The corresponding levels in the DIPM calculation have the same neutron $\nu(f_{7/2}h_{9/2}i_{13/2})$ configuration, while proton configurations are $\pi(h_{11/2}d_{5/2}{}^{-1})$, $\pi(h_{11/2}{}^3d_{5/2}{}^{-1})$ and $\pi(h_{11/2}{}^3d_{5/2}{}^{-3})$. The seniority increases from ν=5 to 9, as excitation energy increases. Just above the high-spin isomer, the states with increasing angular momentum are formed by the proton excitation as same as low-spin states.

4-3. Yrast deformation

The deformations of the yrast states in ^{145}Sm and ^{147}Gd were calculated by a deformed independent particle model (DIPM)[23]. The deformation parameters β of two nuclei are shown as a function of an angular momentum in fig.4-8. The experimental values for isomers in ^{147}Gd taken from ref.17 are also plotted in this figure.

The dramatic increase of deformation from $\beta \sim 0$ to -0.19 occurs at the $49/2^+$ isomer in both nuclei ^{145}Sm and ^{147}Gd. The high-spin isomer is considered to be caused by this sudden shape change from spherical to oblate shape. The configuration of these isomers is deduced to be $\{\pi h_{11/2}{}^2 \nu(f_{7/2}h_{9/2}i_{13/2})\}_{49/2^+}$, by the calculation in ref.23. The large shape change is explained by the fact that the neutron core excitation firstly occurs at the $49/2^+$ state and angular momenta of neutrons are aligned along the symmetry axis.

The yrast deformation of $^{210\sim216}$ Rn[13] as well as the even-even nuclei of Gd, Dy and Er[14] with N=82, 84 and 86 are also calculated using DIPM. The plots of the deformation parameter β versus angular momentum are displayed in fig.4-9. In all plots, the yrast deformations gradually change to oblate as the angular momentum increases. These slopes are also found to be steeper as the decrease of the valence particle number outside the neutron closed shell. The maximum angular momentum built up by alignment of those of the valence particles becomes to be smaller, as the neutron number decreases. Therefore, the large deformation appears at relatively low spin and the slope is steeper for lighter isotopes, because the neutron core excitation starts at smaller angular momentum as the neutron number decreases.

The sudden increase of deformation, which is found in ^{145}Sm and ^{147}Gd, are observed in ^{210}Rn as well as the N=82 isotones of Gd, Dy and Er. In the case of ^{210}Rn with two neutron holes within the neutron closed shell, this deformation

change was explained as follows; Two neutron holes in the high-j orbits favor prolate shape, while proton valence particles favor the oblate shape. They cancel each other and the nucleus has spherical shape. However, at higher spin states than the maximum angular momentum built up by the four valence protons and two neutron holes, the particle-hole neutron core excitation occurs. This core excitation causes the rapid increase of deformation.

In A$\sim$ 150 region, the N=82 isotones of Gd, Dy and Er have 0, 2 and 4 proton particles outside the core which corresponds to the sub-shell closure (Z=64 and N=82), while ^{145}Sm and ^{147}Gd have 2 and 0 proton holes, respectively, and one neutron outside the core. Although they have the different numbers of valence particles and holes, the rapid deformation changes appear when the neutron core excitation occurs. Since the proton number seems not to affect the nuclear shape of these nuclei, this fact may indicate the softness of Z=64 shell closure.

In fig.4-8, the large fluctuations of the deformation both of ^{145}Sm and ^{147}Gd in the region of I$\geq$49/2 are shown. The same fluctuation is also found in fig.4-9(b). These fluctuations are considered to originate from the competition among orbits near Fermi surface which favor spherical and oblate shapes. In these shape competitive region, the level scheme become to be complex as several states with the same spin of different configurations exist near the yrast state.

4-4. Average moment of inertia

The excitation energy of the experimental yrast states of ^{145}Sm and ^{147}Gd are plotted as a function of I(I+1) in fig.4-10. The data of ^{145}Sm and ^{147}Gd are taken from this work and ref.37, respectively. The yrast lines are proportional to I(I+1) on average although the plots indicate the irregularity along straight lines because of single-particle characters. The energies of the $13/2^+$ state in two nuclei lie below the straight lines, because the octupole collectivity is mixed in this state.

In high-spin region, Corioris effect causes the breaking of the pairing correlation and the superfluidity disappears[1]. The Fermi gas model can be applied in this yrast region. The total angular momentum originates from the alignment of individual particle angular momentum along the symmetry axis. Consequently, the excitation energies of the yrast states increase linearly with $\frac{\hbar^2}{2J}$I(I+1) on the average, with the classical rigid body moment of inertia.

On the average, the yrast line of ^{145}Sm is proportional to I(I+1) for whole spin region, while that of ^{147}Gd are divided into two straight lines with the crossing point of the $49/2^+$ spin. By the least square fit to the data, the average moment of inertia $\frac{2J}{\hbar^2}$ is obtained. This value of ^{145}Sm is extracted to be 86 MeV^{-1}. Those of ^{147}Gd are deduced to be 77 MeV^{-1} for $17/2 \leq I \leq 41/2$, and 119 MeV^{-1} for $I \geq 49/2$. The average moment of inertia value of ^{147}Gd is larger in the spin region above the high-spin isomer than in low-spin region.

The rigid body moment of inertia given by

$$J_{\mathrm{rid}} = \frac{2}{5}\mathrm{AMR}_0^2(1+0.6\beta)$$

is calculated for ^{145}Sm and ^{147}Gd in the range of $-0.2 \leq \beta \leq 0$ to be 111$\sim$124 and 114$\sim$128 MeV^{-1}, respectively. Average moments of inertia taken from experiment and rigid body values are listed in Table 4-1.

The experimental value of ^{147}Gd for I$\geq$49/2 is close to the rigid body value. Therefore, it is considered that the pairing correlations disappears rather suddenly at around the $49/2^+$ level, and superfluidity disappeared for I$\geq$49/2. The nuclear shape seems to be oblate in this spin region because the deformation parameter is $\beta<0$ by the DIPM calculation and the experimental value is $\beta=-0.19$ at the $49/2^+$ state.

However, the average moment of inertia of ^{145}Sm is smaller than the rigid body value in all spin region. To understand this difference, it is necessary for ^{145}Sm to determine the level scheme in detail and spin of each levels definitely above the $49/2^+$ high-spin isomer.

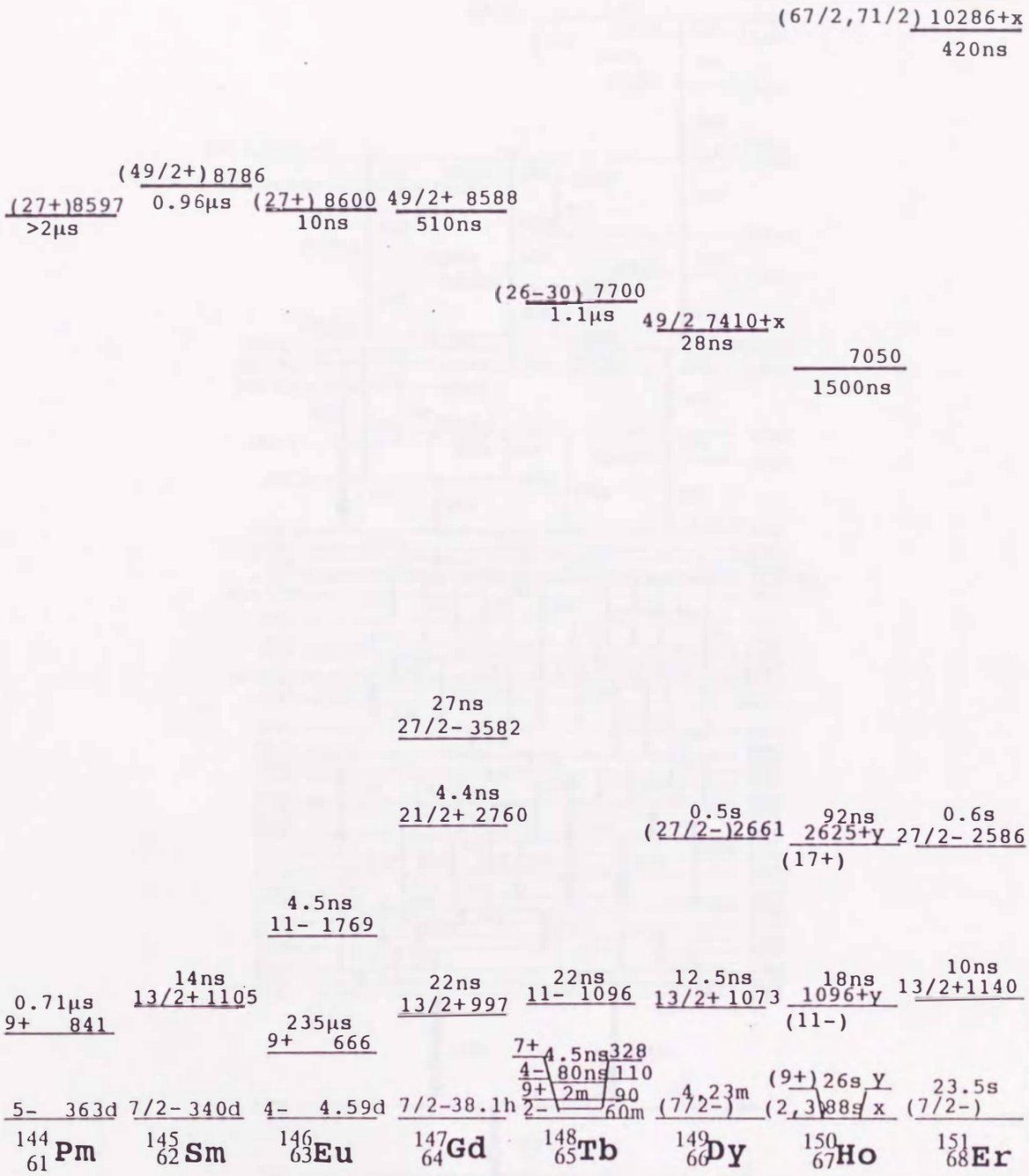

fig.4-1 Systematics of isomers of N=83 isotones. The data of ^{145}Sm is obtained in this work and those of ^{144}Pm, ^{146}Eu, ^{147}Gd, ^{148}Tb, ^{149}Dy, ^{150}Ho and ^{151}Er are taken from refs.35-41, respectively.

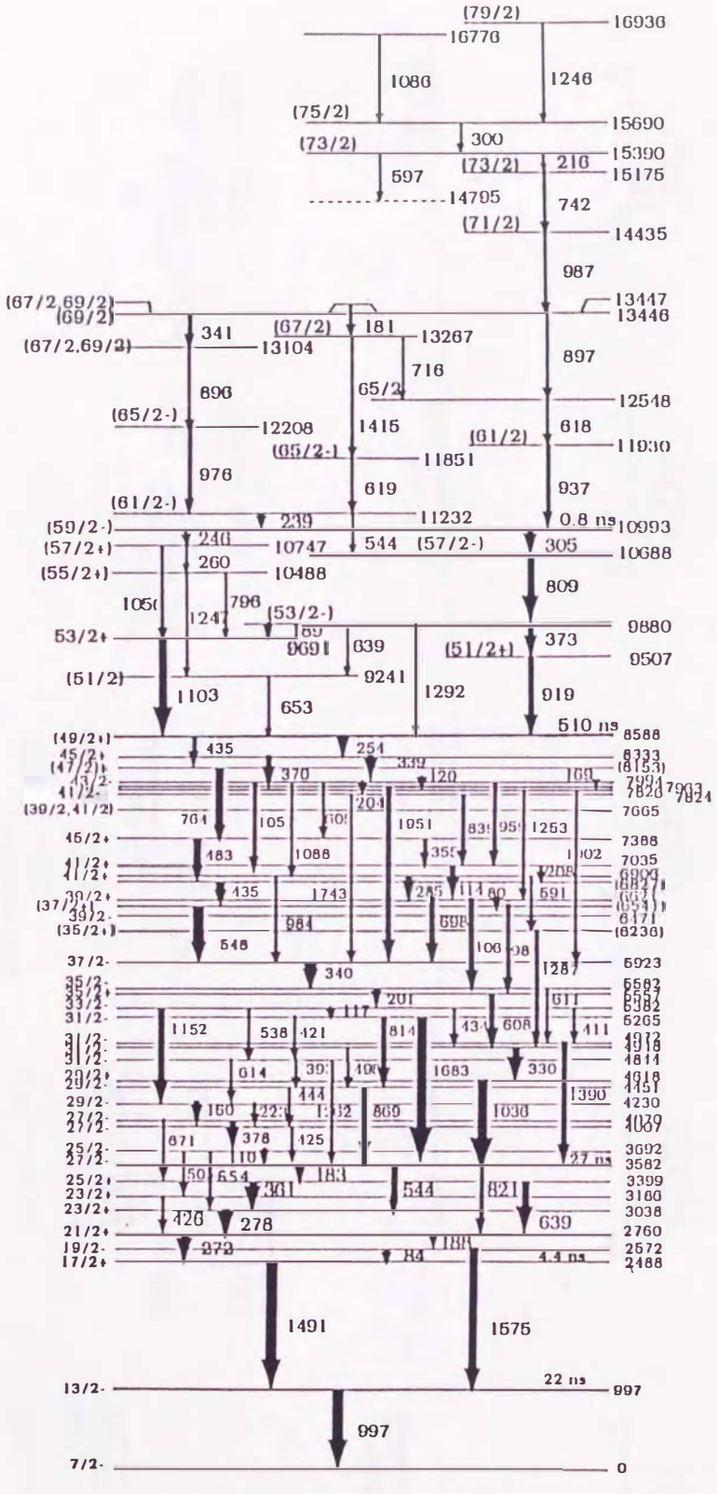

^{147}Gd

fig.4-2 Level scheme of ^{147}Gd taken from ref.37.

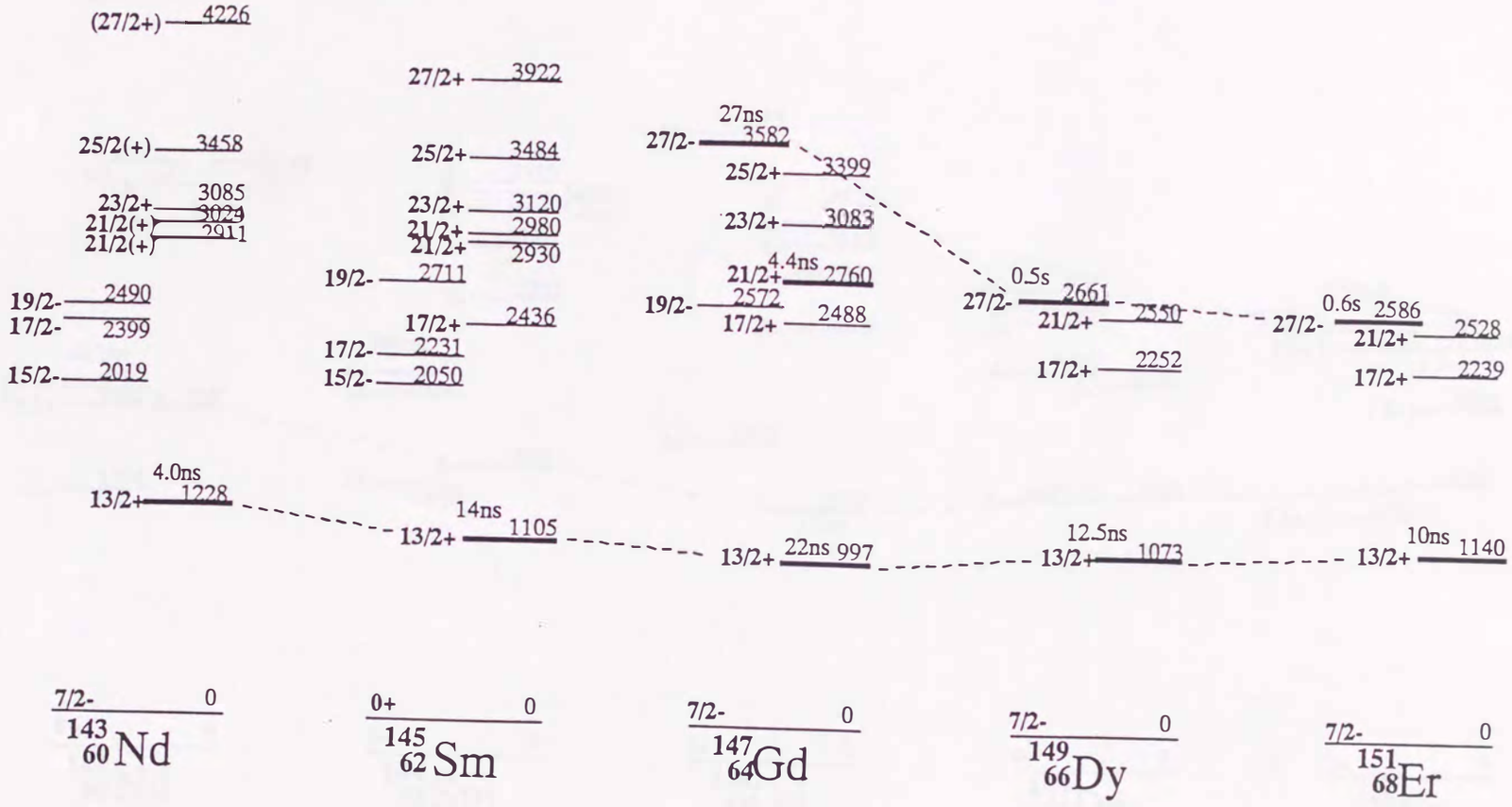

fig.4-3 Level systematics of the N=83 odd isotones. The data of ^{145}Sm is obtained in this work, and those of ^{143}Nd, ^{147}Gd, ^{149}Dy and ^{151}Er are taken from refs.42, 37, 39 and 41, respectively.

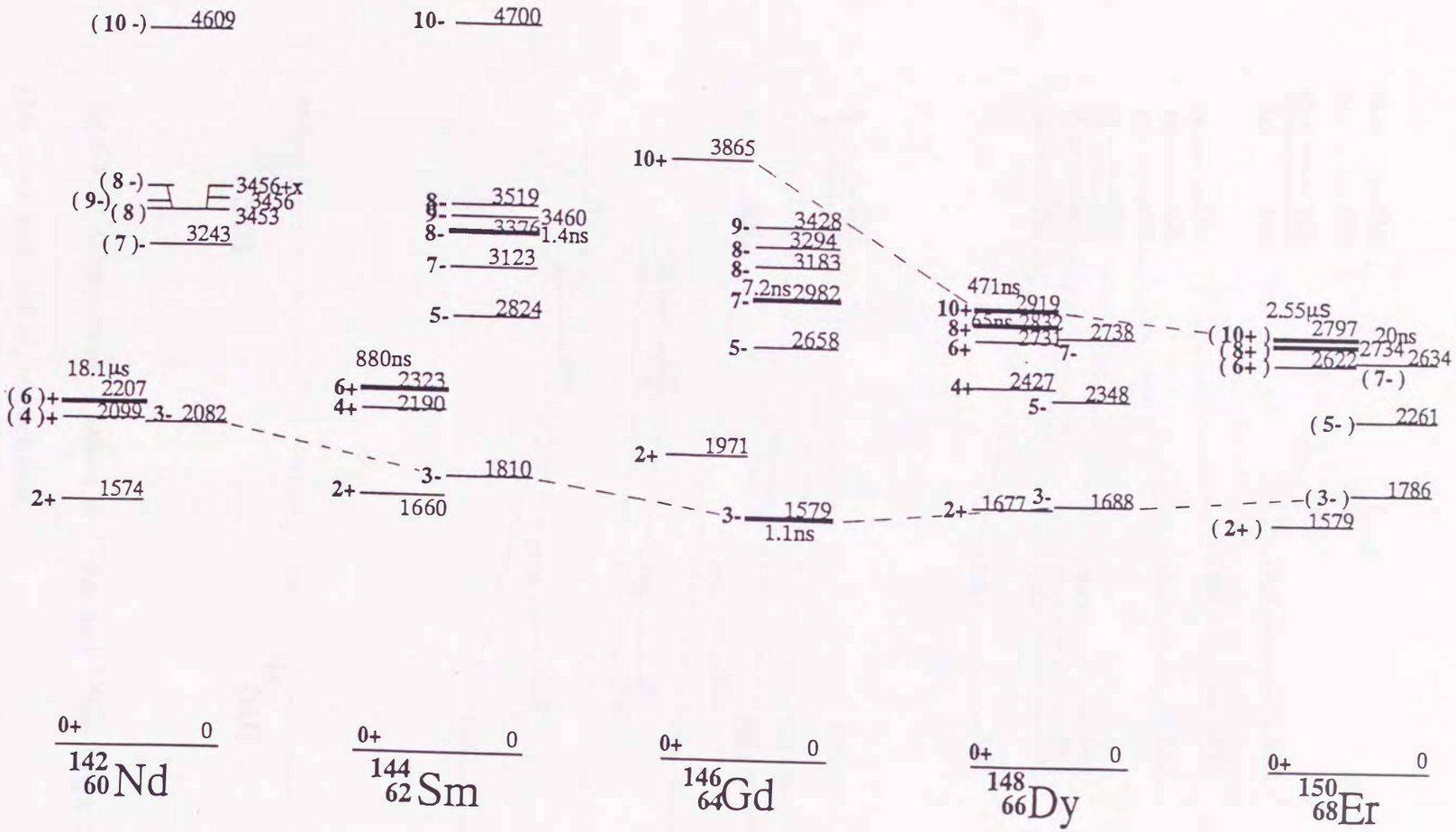

fig.4-4 Level systematics of the N=82 doubly-even isotones. The data of ^{142}Nd, ^{144}Sm, ^{146}Gd, ^{148}Dy and ^{150}Er are taken from refs.43-47, respectively.

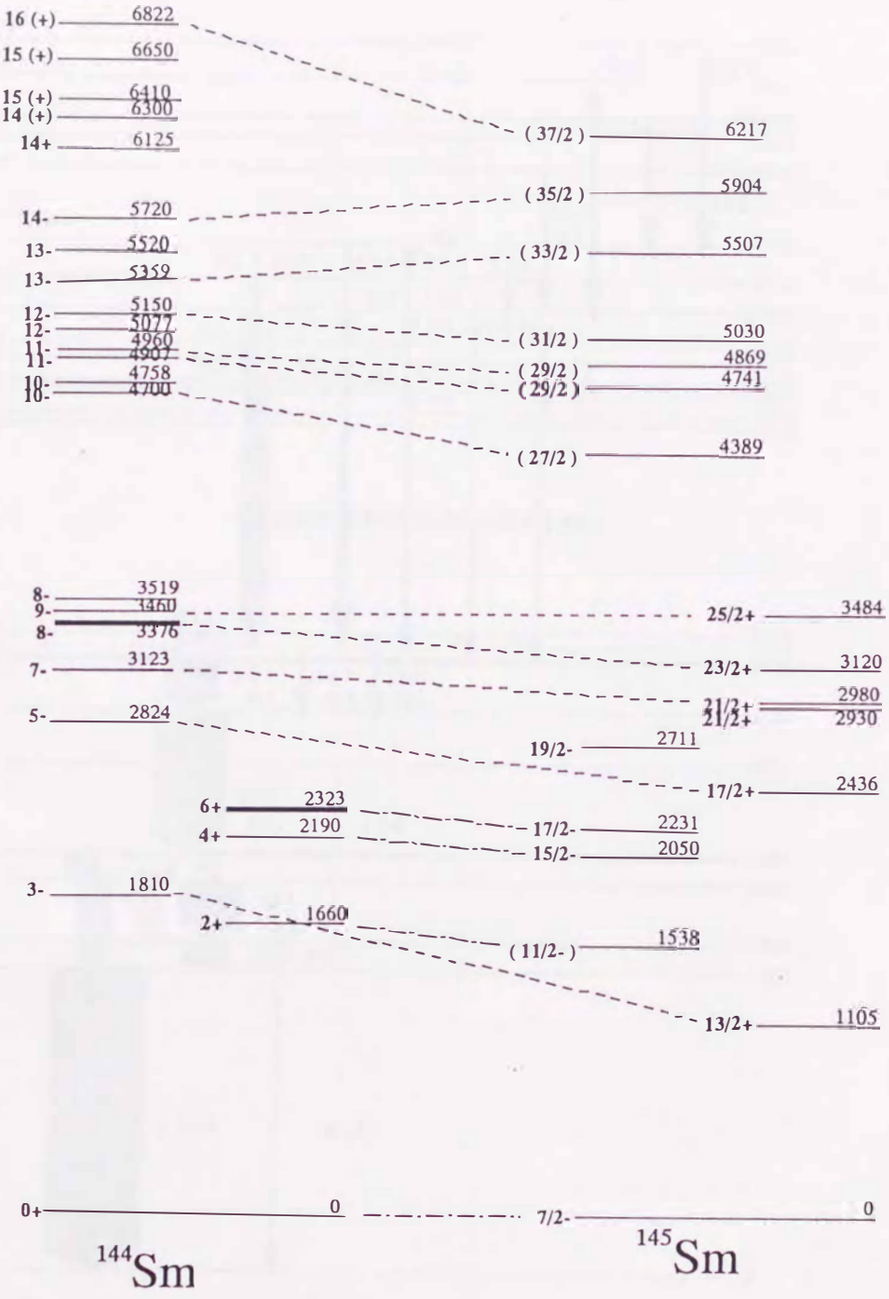

fig.4-5 Comparison of states in ^{145}Sm and ^{144}Sm taken from this work and ref.44, respectively.

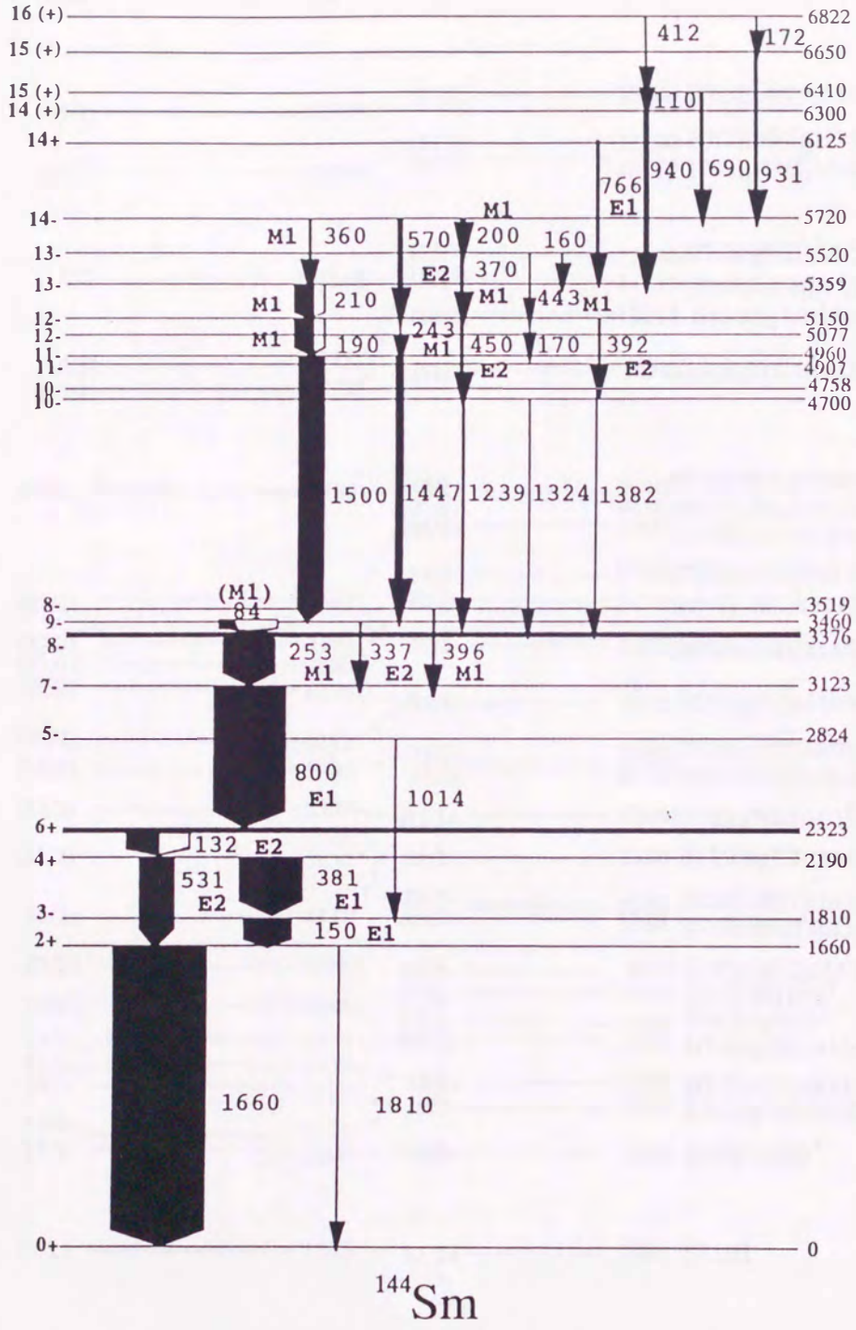

fig.4-6 Level scheme of ^{144}Sm taken from ref.44.

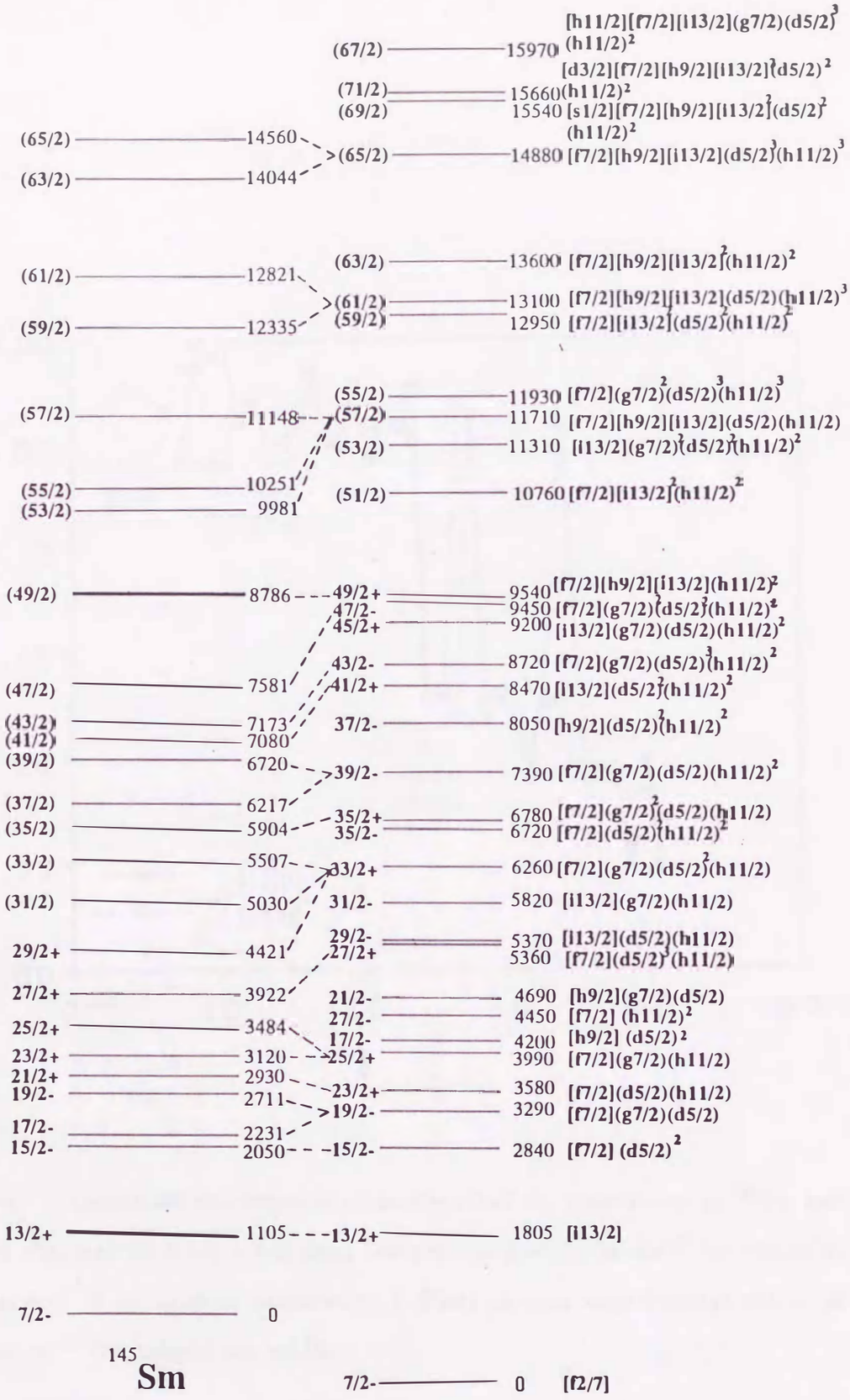

fig.4-7 Experimental yrast states resulted in this work and of the calculation made by using a deformed independent particle model[23].

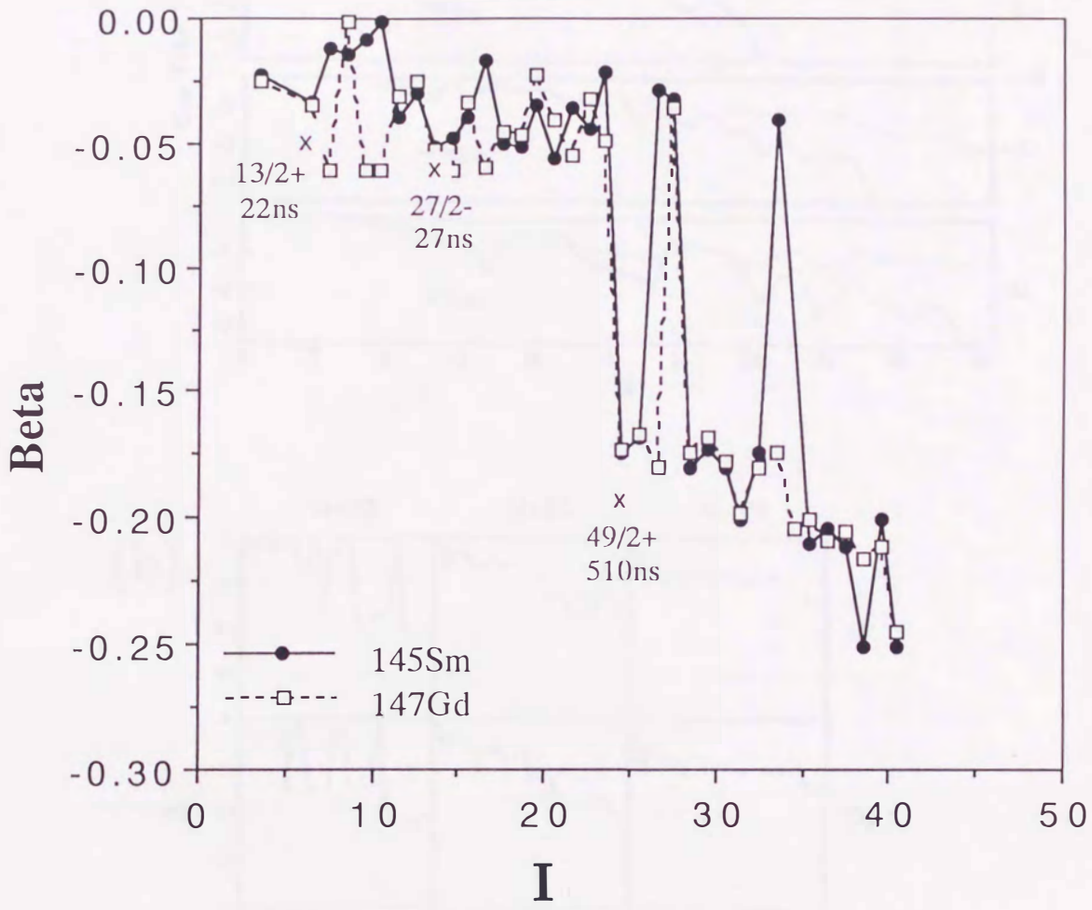

fig.4-8 Calculated deformation parameters β of the yrast states in ^{145}Sm and ^{147}Gd obtained by using a deformed independent particle model[23] are shown as a function of an angular momentum I. Plots present experimental values of isomer in ^{147}Gd, taken from ref.18.

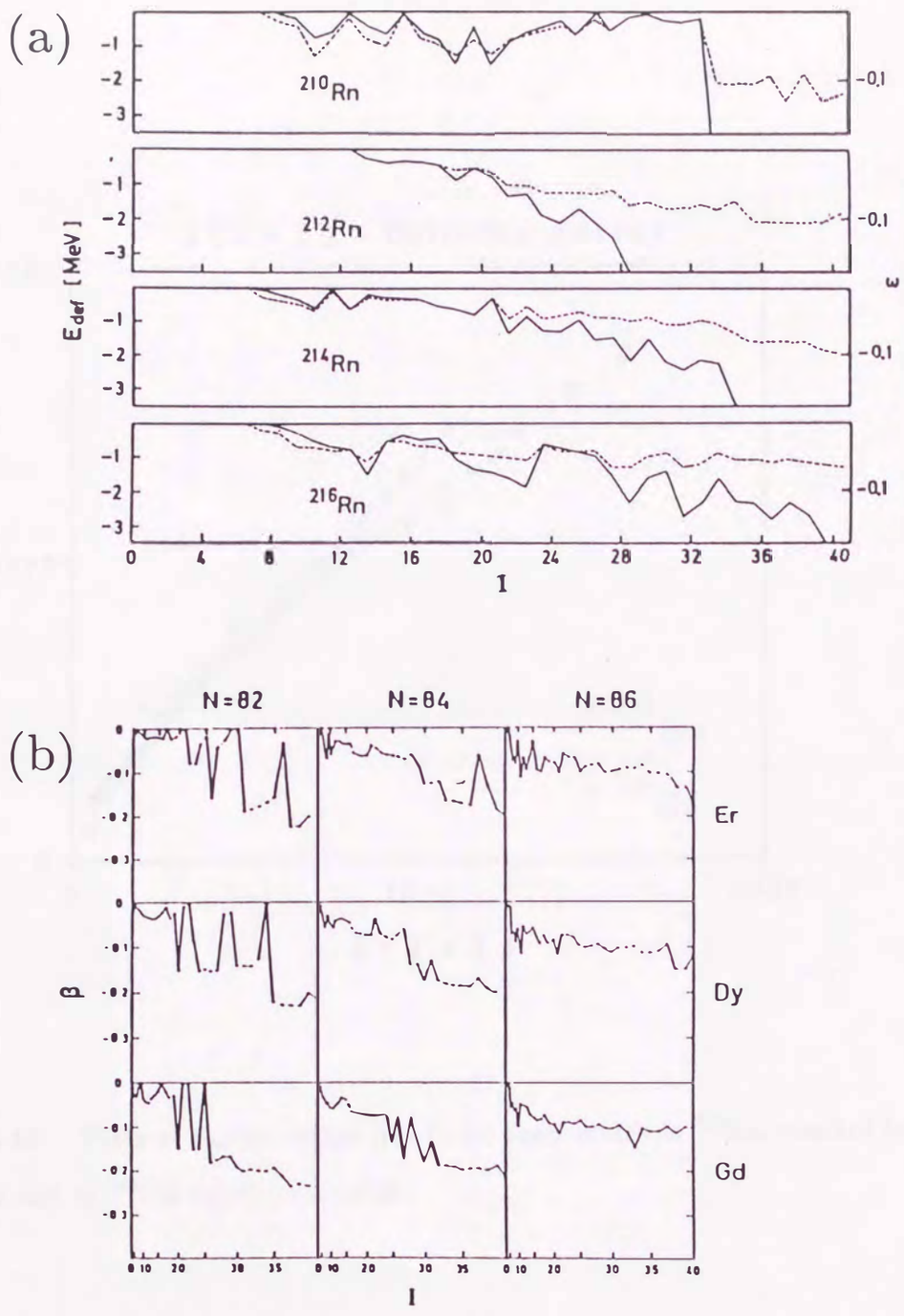

fig.4-9 Calculated deformations β of the yrast states in (a)$^{210\sim216}$Rn and (b)doubly-even nuclei of Er, Dy and Gd with N=82∼86 obtained by using a deformed independent particle model[13−14].

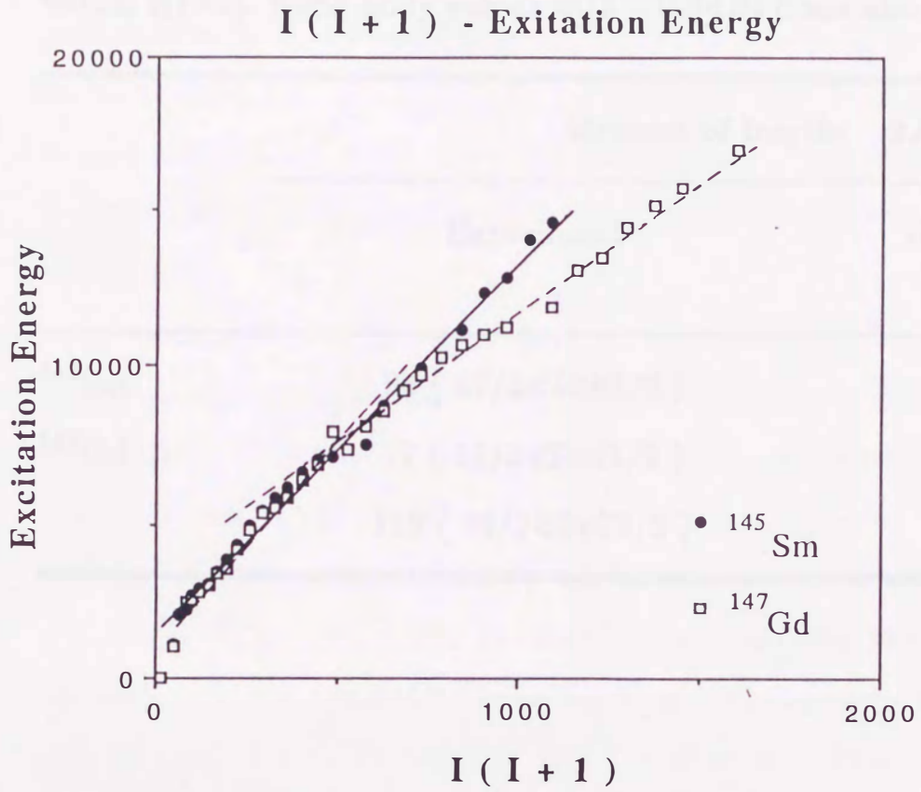

fig.4-10 Plots of energy versus I(I+1) for yrast states in ^{145}Sm resulted in this work and of ^{147}Gd taken from ref.37.

Table 4-1 Average moments of inertia of ^{145}Sm and ^{147}Gd extracted as a slope of the curves in the plots of excitation energies of the levels versus I(I+1). Rigid body values with $-0.2<\beta<0$ are also given.

	Moment of Inertia $2J/\hbar^2$	
	Experiment	rigid body value ($-0.2<\beta<0$)
^{145}Sm	86 (17/2<I<65/2)	111~124
^{147}Gd	77 (17/2<I<41/2)	114~128
	119 (49/2<I<79/2)	

5. Conclusion

The high-spin isomer in ^{145}Sm was discovered. The level scheme was constructed up to the state at 14.6 MeV using the data taken by three different reactions. The excitation energy of this isomer was determined to be 8.8 MeV. The spin assignments were tentatively given based on the γ-ray angular distributions.

The high-spin isomer in ^{145}Sm is similar to that in ^{147}Gd in excitation energies and complex decay paths. The configuration of this isomer is deduced to be $\{\pi h_{11/2}{}^2\nu(f_{7/2}h_{9/2}i_{13/2})\}_{49/2^+}$ by a deformed independent particle model (DIPM) calculation[23].

Low-lying states up to the (35/2) state at 6.0 MeV in ^{145}Sm were interpreted as a single neutron $f_{7/2}$ coupled to the ^{144}Sm core excitation. The configuration of each state is much different from that of ^{147}Gd. Experimental yrast states correspond well with the DIPM calculation.

Variations of yrast deformations as a function of an angular momentum were deduced for ^{145}Sm and ^{147}Gd by the DIPM calculation. These plots were discussed and compared with those of Rn isotopes and of the doubly-even nuclei of Er, Dy and Gd with N=82, 84 and 86. They all show the increase of the oblate deformations as the angular momentum increases. The high-spin isomers in ^{145}Sm and ^{147}Gd seem to be caused by the sudden shape change from near spherical to oblate deformation.

Average moments of inertia of ^{145}Sm and ^{147}Gd were obtained from the plots of excitation energies of the levels versus I(I+1). In case of ^{147}Gd, the moment of inertia extracted as a slope of the curve is close to a rigid body value for $I \geq 49/2$. It is considered that the pairing correlation is broken and superfluidity disappears. On the other hand, the average moment of inertia of ^{145}Sm for $I \geq 49/2$ seems to be the same as that for $I \leq 49/2$.

Acknowledgements

The author would like to thank Prof. Y.Gono for precious advice, stimulating discussion, and encouragement. She is also grateful to Prof. T.Kuroyanagi and Dr. S.Mitarai for their great helps and various guidances. She also thanks the members of the γ-groups in Kyushu University for their support to perform experiments. She would like to acknowledge Profs. S.Morinobu and T.Nakashima for their suggestion and interests in this work, and the members of the Tandem Accelerator in Kyushu University for their help and encouragement. Thanks are due to Mr. T.Maeda and Mr. Y.Koga for preparation of the electronic circuits and experimental apparatus.

The author wishes to express her gratitude to Drs. K.Morita and T.Morikawa as well as collaborators in RIKEN for various discussion and encouragement. She is greatly indebted to Dr. M.Oshima, collaborators and staffs in Japan Atomic Energy Research Institute for their help in performing the experiments at JAERI.

The author must add her thanks to Dr. K.Tanaka of KEK for his supply of the ^{13}C material.

The author wishes to acknowledge Profs. K.Matsuyanagi and H.Sagawa for their calculations of a deformed independent particle model and theoretical discussions. She is thankful to Prof. K.Takada and Dr. Y.R.Shimizu for their theoretical support.

The author is much indebted to late Dr. N.Kato for his advice, help and kindness during his last year.

Finally, the author is really thankful to her family for their support to accomplish this thesis work.

References

1. A.Bohr and B.R.Mottelson, Phys. Scr. **10A**(1974)13

2. J.Pedersen, B.B.Back, F.M.Bernthal, S.Bjørnholm, J.Borggreen, O.Christensen, F.Folkmann, B.Herskind, T.L.Khoo, M.Neiman, F.Pühlhofer, and G.Sletten, Phys.Rev.Lett. **39**(1977)990

3. A.Faessler, M.Ploszajzac and K.R.S.Devi, Phys.Rev.Lett. **26**(1976)1028

4. M.Ploszajczak, A.Faessler, G.Leander and G.Nilsson, Nucl.Phys. **A301**(1978)477

5. R.Bengtsson, S.E.Larsson, G.Leander, P.Möller, S.G.Nilsson and S.Åberg, Phys.Lett.**B57**(1975)301

6. M.Cerkaski, J.Dudek, Z.Szymański, G.G.Andersson, G.Leander, S.Åberg, G.Nilsson and I.Pagnarsson, Phys.Lett. **B70**(1977)9

7. G.Andersson, S.E.Larsson, G.Leander, P.Möller, S.G.Nilsson, I.Pagnarsson, S.Åberg, R.Bengtsson, J.Dudek, B.Nerlo-Pomorska, K.Pomorskiand Z.Szymański, Nucl.Phys. **A268**(1976)205

8. C.G.Andersson and J.Klumlinde, Nucl.Phys.**A291**(1977)

9. C.G.Andersson, G.Hellstrom, G.Leander, I.Pagnarsson, S.Åberg, j.Klumlinde, S.G.Nilsson and Z.Szymański, Nucl.Phys. **A309**(1978)141

10. K.Neergård, V.V.Pashkevich and S.Frauendorf, Nucl.Phys. **A262**(1976)61

11. K.Neergård, H.Toki, M.Ploszajczak and A.Faessler, Nucl.Phys. **A287**(1977)48

12. T.Døssing, K.Neergård, K.Matsuyanagi and Hs.-Ch.Chang, Phys.Rev.Lett.**39**(1977)1195

13. K.Matsuyanagi, T.Døssing and K.Neergård, Nucl.Phys. **A307**(1978)253

14. T.Døssing, K.Neergård and H.Sagawa, Phys.Scr. **24**(1981)258

15. R.Broda, P.Kleinheinz, S.Lunardi, J.Styczen and J.Bronquist, Z.Phys. **A305**(1982)281

16. O.Bakander, C.Baktash, J.Borgreen, J.B.Jensen,K.Kownacki, J.Pedersen, G.Sletten, D.Ward, H.R.Andrews, O. Häusser, P.Skensved and P.Taps, Nucl.Phys. **A389**(11982)93

17. O.Häusser, P.Taras, W.Trautman, D.Ward, T.K.Alexander, H.R.Andrews, B.Haas and D.Horn, Phys.Rev.Lett. **42**(1979)1451

18. O.Häusser, H.E.Mahnke, T.K.Alexander, H.R.Andrews, J.F.Sharpey-Scharfer, M.L.Swanson, D.Ward, P.Taras and Keinonen, Nucl.Phys. A379(1982)287
E.Dafni, J.Bendahan, C.Broude, G.Goldring, M.Hass, E.Naim, M.H.Rafailovich, C.Chasman, O.C.Kistner and S.Vajda, Nucl.Phys. **A443**(1985)135

19. M.Drigert, M.Piiparinen, R.V.F.Janssens, R.Holzmann, I.Ahmad, J.Borggreen, R.R.Chasman, P.J.Daly, B.K.Dichter, H.Emling, U.Garg, Z.W.Grabowski, T.L.Khoo, W.C.Ma, M.Quader, D.C.Radford and W.Trzaska, Nucl.Phys. **A515**(1990)466

20. K.Zuber, D.Balouka, F.A.Beck, Th,Byrski, D.Curien, G.Duchene, C.Gehringer, B.Haas, J.C.Merdinger, P.Romain, D.Santos, J.P.Vivien, J.Dudek, Z.Szymański and T.Werner, Nucl.Phys.**A520**(1990)195c

21. P.Kleinheinz, M.Ogawa, R.Broda, P.J.Daly, D.Haenni, H.Beuscher and A.Klinrahm, Z.Phys. A286(1978)27

22. M.Ogawa, R.Broda, K.Zell, P.j.Daly and P.Kleinheinz, Phys.Rev.Lett.**41**(1978)289

23. H.Sagawa, Private communication

24. K.Matsuyanagi, Private communication

25. G.Hackman, S.M.Mullins, J.A.Kuehner, D.Prévost, J.C.Waddington, A.Galindo-Uribarri, V.P.Janzen, D.C.Radford, N.Schmeing and D.Ward, Phys.Rev. **C47**(1993)R433

26. M.Piiparinen, Y.Nagai, P.Kleinheinz, M.C.Bosca, B.Rubio, M.Lach and J.Blomquist, Z.Phys. A-Hadrons and Nuclei **338**(1991)417

27. P.Kleinheinz, M.R.Maier, R.M.Diamond, F.S.Stephens and R.K.Sheline, Phys.Lett. **B53**(1975)442

28. Z.Haratym, J.Kownacki, J.Ludziejewski, Z.Sujkowski, L.-E. de Geer, A.Kerek and H.Ryde, Nucl.Phys. **A276**(1977)299

29. I.Adam, K.S.Toth and F.Roche, Nucl.Phys. A121(1968)289
E.Newman, K.S.Toth and I.R.Wiliams, Phys.Rev. **C7**(1973)290

30. W.Booth, S.Wilson and S.S.Ipson, Nucl.Phys. A229(1974)61
W.Booth and S.Wilson, Nucl.Phys. **A247**(1975)126

31. H.Kader, G.Graw, F.J.Eckle, G.Eckle, P.Schiemenz, P.Kleinheinz, B.Rubio, G.de Angelis, T.N.Massey, L.G.Mann and J.Blomquist, Phys.Lett. **B227**(1989)325

32. Y.Gono, T.Murakami, T.Morikawa, A.Ferragut, Y.H.Zhang, K.Morita, A.Yoshida, H.Kumagai, M.Oshima, H.Kusakari, M.Sugawara, M.Ogawa, M.Nakajima, S.Mitarai, A.Odahara, E.Ideguchi, T.Shizuma, M.Kidera, J.C.Kim, S.J.Chae and B.J.Min, Nucl.Phys. **A557**(1993)341c

33. A.Ferragut, Y.Gono, T.Murakami, T.Morikawa, Y.H.Zhang, K.Morita, A.Yoshida, M.Oshima, H.Kusakari, M.Sugawara, M.Ogawa, M.Nakajima, S.Mitarai, A.Odahara, E.Ideguchi, T.Shizuma, M.Kidera, J.C.Kim, S.J.Chae, B.J.Min and H.Kumagai, J.Phys.Soc.Jpn. **62**(1993)3343

34. T.Sugimitsu, N.Kato, Y.Koga, T.Maeda, S.Mitarai, T.Okamoto, J.Mukai, S.Niiya, A.Odahara, T.Mukae, E.Ideguchi, S.Mitsuoka, K.Utsunomiya, T.Shizuma, M.Hijiya and K.Nakamoto, KUTL Rep.(1991-1992)164

35. T.Murakami, Y.Gono, A.Ferragut, Y.H.Zhang, K.Morita, A.Yoshida, M.Ogawa, M.Nakajima, B.J.Min, H.Kumagai, M.Oshima, T.Morikawa, M.Sugawara and H.Kusakari, Z.Phys. **A345**(1993)123

36. E.Ideguchi, T.Morikawa, Y.Gono, S.Mitarai, A.Odahara, M.Kidera, M.Shibata, M.Oshima, Bull.Phys.Soc.Jpn. (1993)108

37. E.der Mateosian and L.K.Peker, Nucl.Data Sheets **66**(1992)705

38. L.K.Peker, Nucl.Data Sheets **59**(1990)303

39. J.A.Szűcs, M.W.Johns and B.Singh, Nucl.Data Sheets **46**(1985)1

40. J.B.Borggreen, S.Bjonholm, O.Christensen, A.Del Zoppo, B.Herskind, J.Pedersen, G.Sletten, F.DFolkmann, R.S.Simon, Z.Phys. **A294**(1980)113

41. S.André, C.Foin, V.Barci, D.Barnéound, J.Genevey and A.Gizon, Z.Phys. **A337**(1990)349

42. L.K.Peker, Nucl.Data Sheets **63**(1991)647

43. L.K.Peker, Nucl.Data Sheets **48**(1986)753

44. M.Ogawa, Private communication

45. L.K.Peker, Nucl.Data Sheets **60**(1990)953

46. L.K.Peker, Nucl.Data Sheets **59**(1990)393

47. Y.H.Chung, P.J.Daly, H.Helppi, R.Broda, Z.W.Grabowski, M.Kortelahti, J.McNeill, A.Pakkanen, P.Chowdhury, R.V.F.Janssens, T.L.Khoo and J.Blomquist, Phys.Rev. **C29**(1984)2153

48. J.H.McNeill, A.A.Chishti, P.J.Daly, W.Gellently, M.A.C.Hotchkis, M.Piiparinen, B.J.Varley, P.J.Woods and J.Blomquist, Z.Phys. **A 344**(1993)369

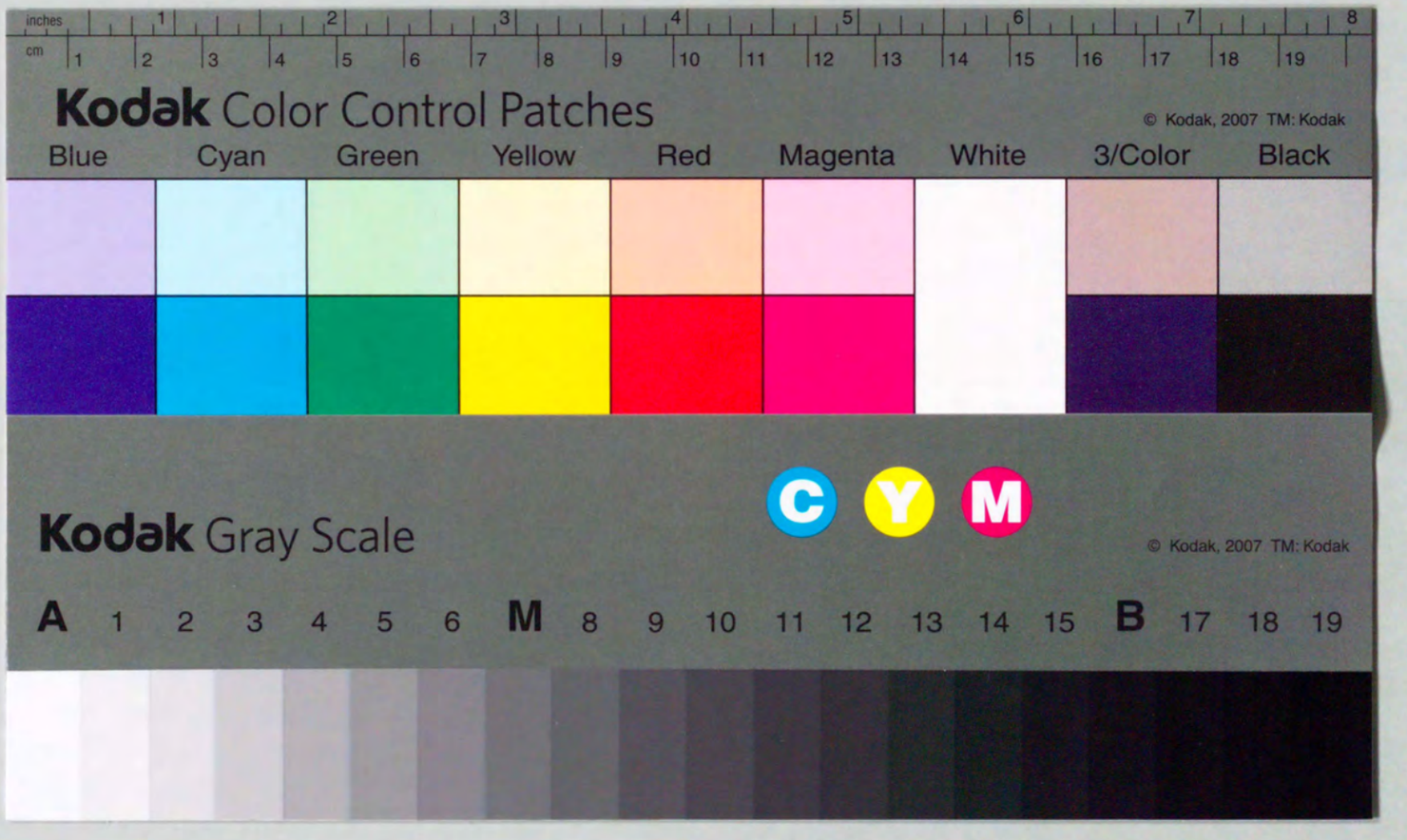
inches
cm
Kodak Color Control Patches
© Kodak, 2007 TM: Kodak
Blue
Cyan
Green
Yellow
Red
Magenta
White
3/Color
Black
Kodak Gray Scale
C
Y
M
© Kodak, 2007 TM: Kodak
A 1 2 3 4 5 6 M 8 9 10 11 12 13 14 15 B 17 18 19